

Supporting Information

Direct Observation of Oxygen Rebound with an Iron-Hydroxide Complex

Jan Paulo T. Zaragoza,¹ Timothy H. Yosca,² Maxime A. Siegler,¹ Pierre Moënne-Loccoz,³
Michael T. Green,² and David P. Goldberg^{1*}

¹Department of Chemistry, The Johns Hopkins University, 3400 N Charles Street, Baltimore, Maryland 21218.

²Department of Chemistry and Department of Molecular Biology and Biochemistry, University of California, Irvine, California 92697.

³Division of Environmental and Biomolecular Systems, Oregon Health & Science University, Portland, Oregon 97239.

Experimental Details

Materials. All chemicals were purchased from commercial sources and used without further purification unless otherwise stated. Reactions involving inert atmospheres were performed under an Ar atmosphere using standard Schlenk techniques or in an N₂-filled dry box. Toluene, dichloromethane, acetonitrile, and diethyl ether were purified via a Pure-Solv solvent purification system from Innovative Technologies, Inc. Ethyl acetate and toluene were dried by distilling over CaH₂. Deuterated solvents for NMR and ⁵⁷Fe (95.93%) were purchased from Cambridge Isotopes, Inc. Solvents were degassed by repeated cycles of freeze–pump–thaw and stored over 4 Å molecular sieves in an N₂-filled drybox prior to use. ⁵⁷FeCl₂ (⁵⁷Fe 95.93%) was synthesized using a previously published method.¹ Tris(*p*-*t*-butylphenyl)methyl bromide,² tris(*p*-phenylphenyl)methanol³ and tris(*p*-phenylphenyl)methyl bromide⁴ were synthesized following previously reported procedures. Tris(*p*-methoxyphenyl)methyl chloride and tris(*p*-chlorophenyl)methanol were obtained from Alfa-Aesar and were used as received. The triphenylmethyl radical source, Gomberg’s dimer ((Ph₃C)₂) was synthesized following literature procedures.⁵⁻⁶

Instrumentation. Kinetics and other UV-vis measurements were performed on a Hewlett-Packard Agilent 8453 diode-array spectrophotometer with a 3.5 mL quartz cuvette (path length = 1 cm) fitted with a septum. For reactions with total reaction time of <10 seconds, stopped-flow experiments were carried out using a HiTech SHU-61SX2 (TgK scientific Ltd.) stopped-flow spectrophotometer with a xenon light source and Kinetic Studio software. Laser desorption ionization mass spectrometry (LDI-MS) was conducted on a Bruker Autoflex III Maldi ToF/ToF instrument (Billerica, MA) equipped with a nitrogen laser at 335 nm using an MTP 384 ground steel target plate. The instrument was calibrated using peptide standards of known molecular weights. Electrospray ionization mass spectra (ESI-MS) were acquired using a Finnigan LCQ Duo ion-trap mass spectrometer equipped with an electrospray ionization source (Thermo Finnigan, San Jose, CA) in positive ion mode. Samples were dissolved in 1:1 CH₂Cl₂/CH₃CN and introduced into the instrument at a rate of 25 μL/min using a syringe pump via a silica capillary line. The heated capillary temperature was 110 °C and the spray voltage was 4 kV. Gas Chromatography (GC-FID) was carried out on an Agilent 6850 gas chromatograph fitted with a DB-5 5% phenylmethyl siloxane capillary column (30 m x 0.32 mm x 0.25 μm) and equipped with a flame-ionization detector. Gas chromatography mass spectrometry (GC-MS) was performed using a Shimadzu GC17A/QP5050A GC/MS combination (Shimadzu Instruments, Columbia, MD). The GC17A is equipped with a low polarity (5% phenyl-, 95% methyl-siloxane) capillary column (30 m length, 0.25 mm ID, 0.25 μm film thickness, 10 m length guard column). Samples were dissolved in toluene at a concentration of 2 mM and were injected into the instrument using an autosampler. The QP5050A is an EI quadrupole based mass spectrometer with a maximum scan range of 900 amu and an ionizing electron energy of 70eV. ¹H NMR spectra were recorded on a Bruker Avance 400 MHz NMR spectrometer at 298 K, and referenced against residual proton signals. Elemental analyses were performed at Atlantic Microlab, Inc., Norcross, GA. Electron paramagnetic resonance (EPR) spectra were recorded with a Bruker EMX spectrometer equipped with a Bruker ER 041 X G microwave bridge and a continuous-flow liquid helium cryostat (ESR900) coupled to an Oxford Instruments TC503 temperature controller for low temperature data collection. Mössbauer spectra were recorded from a WEB Research (Edina, MN) spectrometer in constant acceleration mode with

transmission geometry. Spectra were recorded with a 53 mT magnetic field applied parallel to the γ -beam. All measurements were recorded at 4.2 K using a Janis SVT400 cryostat. Isomer shifts were calibrated relative to the centroid of the spectrum of a metallic foil of α -Fe at room temperature. Data analysis was performed using the program WMOSS from WEB research. Cyclic voltammetry was performed on an EG&G Princeton Applied Research potentiostat/galvanostat model 263A with a three-electrode system consisting of a glassy carbon working electrode, a Ag/AgNO₃ non-aqueous reference electrode (0.01 M AgNO₃ with 0.1 M Bu₄N⁺PF₆⁻ in CH₃CN), and a platinum wire counter electrode. Potentials were referenced using an external ferrocene standard. Scans were run under an Ar atmosphere at 23 °C using Bu₄N⁺PF₆⁻ (0.1 M) as the supporting electrolyte. Resonance Raman spectra were collected using a custom McPherson 2061/207 spectrograph with a 0.6 focal length and a 2400 grooves per millimeter holographic grating and a liquid-nitrogen cooled CCD detector (LN-1100PB, Princeton Instruments). Samples were probed using a backscattering geometry with the 407 nm laser excitation from a Kr laser (Innova 302 C, Coherent). A long-pass filter (RazorEdge, Semrock) was used to attenuate the Rayleigh scattering. Frequencies were calibrated relative to aspirin and are accurate to within ± 1 cm⁻¹.

5,10,15-Tris(2,4,6-triphenylphenyl)corrole) (tppcH₃). The metal-free ligand was synthesized and purified by slight modification of a previously published procedure.⁷ To a mixture of 2,4,6-triphenylbenzaldehyde⁸ (1 g, 2.99 mmol) and pyrrole (25 mL) was added trifluoroacetic acid (TFA) (50 μ L) and the mixture was stirred for 3 h until a dark red solution was obtained. Triethylamine (300 μ L) was added to quench the reaction, after which the solution turned dark green, and the excess pyrrole was removed by vacuum distillation. The crude 2,4,6-triphenylphenyl dipyrromethane was dissolved in dichloromethane (50 mL) and was added to a solution of 2,4,6-triphenylbenzaldehyde (200 mg, 0.6 mmol) in dichloromethane (200 mL). TFA (25 μ L) was added and the solution was stirred for 3 h before triethylamine (0.15 mL) was added. A solution of DDQ (0.8 g, dissolved in 10 mL THF, then diluted with dichloromethane to 80 mL) was added dropwise using an addition funnel. The solution was dried, and tppcH₃ was purified by column chromatography (4:1 CH₂Cl₂/hexanes, silica), eluting out as the first green band (108 mg, 15% yield). ¹H NMR (400 MHz, CDCl₃) δ (ppm): 8.45 (d, 2H), 8.41 (d, 2H), 8.20 (t, 4H), 7.95 (d, 12H), 7.60 (t, 6H), 7.49 (t, 3H), 6.97 (d, 8H), 6.74 (d, 4H), 6.60 (t, 4H), 6.51 (t, 10H), 6.36 (t, 4H). All other characterization data match the literature values.⁷

Fe^{IV}(Cl)(tppc) (1). To a solution of tppcH₃ (216 mg, 0.18 mmol) in N,N-dimethylformamide (DMF) (50 mL) was added FeCl₂ (450 mg, 3.50 mmol) and the solution was heated to 130 °C for 3 h under Ar. The solvent was removed by vacuum distillation. The product was redissolved in CH₂Cl₂ and initially purified by column chromatography on silica gel (Et₂O, R_f = 0.90) to remove unreacted Fe salts. The resulting brown solid was further purified by column chromatography on silica gel (8:2 CH₂Cl₂/hexanes, R_f = 0.50) to obtain **1** as a pure brown solid (200 mg, 86% yield). Crystals suitable for X-ray diffraction (XRD) were obtained by layering a CH₂Cl₂ solution of **1** with Et₂O and slow evaporation for one week, yielding dark brown blocks of **1**. UV-vis (CH₂Cl₂): λ_{\max} , nm ($\epsilon \times 10^{-4}$ M⁻¹ cm⁻¹): 370 (2.80), 405 (3.25), 514 (1.35), 635 (0.35). ¹H NMR (400 MHz, CD₂Cl₂) δ (ppm): 8.68 (d), 8.46 (d), 8.23 (t), 8.11 (t), 7.32 (t), 7.27 (t), 7.11 (s, br), 6.89 (s, br), 6.71 (s, br), 4.56 (s, br), 3.25 (s, br), -4.07 (s, br), -5.51 (s), -5.82 (s), -7.65 (s), -8.97 (s, br), -35.59 (s, br). LDI-MS (m/z): isotopic cluster centered at 1263.4 (M-Cl)⁺ (calcd 1263.4). ESI-MS (m/z): isotopic cluster centered at 1299.4 (M+H)⁺ (calcd

1299.3). Anal. Calcd for C₉₁H₅₉ClFeN₄: C, 84.09; H, 4.58; N, 4.31. Found: C, 84.01; H, 4.58; N, 4.32.

Fe^{IV}(OH)(ttppc) (2). To a solution of **1** (16.5 mg, 13.1 μmol) in toluene (5 mL) was added an aqueous solution of LiOH (5% w/v, 5 mL), and the biphasic solution was stirred for 3 h, after which completion of the reaction was observed by UV-vis spectroscopy. The toluene layer was extracted, washed with water (3 x 5 mL), and dried over anhydrous sodium sulfate. The solvent was evaporated, and the brown residue was dissolved in ethyl acetate (5 mL) and passed through a short plug of Celite[®]. Crystals suitable for XRD were obtained by vapor diffusion of this solution with *n*-pentane after 1 week, giving **2** as brown blocks (13.0 mg, 77% yield). UV-vis (CH₂Cl₂): λ_{max}, nm (ε x 10⁻⁴ M⁻¹ cm⁻¹): 395 (4.20), 628 (0.42); (toluene): λ_{max}, nm (ε x 10⁻⁴ M⁻¹ cm⁻¹): 403 (3.95), 630 (0.39). ¹H NMR (400 MHz, benzene-*d*₆) δ (ppm): 8.33 (d), 7.86 (s), 6.95 (s, br), 6.75 (s), 6.61 (s, br), 4.61 (s, br), 2.40 (s, br), -1.11 (s, br), -2.84 (s), -3.45 (s), -4.28 (s, br), -5.01 (s), -5.32 (s), -18.14 (s, br). LDI-MS (m/z): isotopic cluster centered at 1280.4 (M⁺) (calcd 1280.4). Anal. Calcd for C₉₁H₆₀FeON₄•EtOAc: C, 83.32; H, 5.01; N, 4.09. Found: C, 83.18; H, 4.92; N, 4.22.

Fe^{III}(OEt₂)₂(ttppc) (3•2Et₂O). To a solution of **1** (18 mg, 14 μmol) in 1:1 ethyl acetate/Et₂O was added Cr(C₆H₆)₂ (4.3 mg, 21 μmol), and the solution was stirred for 10 min. A color change from brown to dark red was observed. This crude mixture was purified by flash column chromatography on silica gel (Et₂O) and dried to obtain **3•2Et₂O** as a dark red solid (15.8 mg, 81% yield). UV-vis (EtOAc): λ_{max}, nm (ε x 10⁻⁴ M⁻¹ cm⁻¹): 420 (4.76), 575 (1.17), 765 (0.25); ¹H NMR (400 MHz, benzene-*d*₆) δ (ppm): 18.44 (s, br), 12.25 (s), 10.84 (s), 8.24 (s), 7.65 (s), 7.42 (s), 6.00 (s, br), 5.42 (s, br), 4.93 (s, br), 1.30 (s, br), 0.92 (s, br), 0.29 (s), -0.96 (s, br), -3.06 (s, br), -3.63 (s, br), -4.31 (s, br), -5.14 (s, br), -5.50 (s, br), -6.15 (s, br), -19.32 (s, br), -60.47 (s, br), -67.31 (s, br). LDI-MS (m/z): isotopic cluster centered at 1263.4 (M⁺). Anal. Calcd for C₉₁H₅₉FeN₄•2Et₂O: C, 84.18; H, 5.64; N, 3.97. Found: C, 84.46; H, 5.99; N, 4.48.

tris(*p*-chlorophenyl)methyl bromide. Following the procedure reported for tris(*p*-butylphenyl)methyl bromide,² tris(*p*-chlorophenyl)methanol (500 mg, 1.37 mmol) was combined with freshly distilled acetyl bromide (5 mL). The reaction mixture was refluxed for 12 h. The remaining acetyl bromide was removed by vacuum distillation, and the solid was washed with petroleum ether. A white solid (460 mg, 79% yield) was obtained. ¹H NMR (400 MHz, toluene-*d*₈): δ (ppm): 6.94 (s, 2H), 6.92 (s, 4H), 6.90 (s, 4H), 6.88 (s, 2H).

Synthesis of trityl radical derivatives (*p*-X-C₆H₄)₃C•. These derivatives exist exclusively as monomers in solution,⁹ and thus should be generated *in situ*. Difficulty in producing high yields of radical solutions at concentrations >10 mM limited the practical radical concentration range in certain cases. *Caution: trityl radicals are O₂ and light-sensitive and care should be taken to avoid exposure of radical solutions to air and light.*

(*p*-OMe-C₆H₄)₃C•. An amount of tris(*p*-methoxyphenyl)methyl chloride (4.89 mM) and excess copper (Cu) powder was added to a scintillation vial in the glove box. Toluene (5 mL) was added to the mixture and was stirred at 75 °C in the dark for 1 h. The red-orange solution was allowed to cool to 23 °C and then filtered through a Celite[®] plug and used immediately for kinetics experiments. UV-vis (toluene): λ_{max}, nm (ε, M⁻¹ cm⁻¹): 536 (570). Radical yield (EPR) =

2.52 mM, 52%. The yield was determined by quantification of the radical concentration by EPR spectroscopy at 23 °C (parameters: frequency = 9.78 GHz, power = 0.2 mW, receiver gain = 5.02×10^4 , mod freq = 100 kHz, mod amp = 0.1 G). The EPR signal ($g = 2.00$) was quantified by double integration and comparison with a TEMPO radical standard calibration curve under non-saturating conditions. The extinction coefficient was calculated using Beer's Law, $\epsilon = A/bc$, where A is the absorbance of the stock solution in toluene at maximum wavelength determined by UV-vis spectroscopy, b is the path length of the UV-vis cuvette (1 cm), and c is the total radical concentration in M.

(*p*-tBu-C₆H₄)₃C•. As previously reported,² an amount of tris(*p*-t-butylphenyl)methyl bromide (4.17 mM) and excess zinc (Zn) powder was added to a scintillation vial in the glove box. Toluene (5 mL) was added to the mixture and was stirred at 23 °C in the dark for 3 h. The yellow solution was filtered through a Celite[®] plug and used immediately for kinetics experiments. UV-vis (toluene): λ_{max} , nm (ϵ , M⁻¹ cm⁻¹): 525 (750). Radical yield (EPR) = 3.61 mM, 87 %. The extinction coefficient obtained from the EPR method is in excellent agreement with a previously reported value of 750(20) M⁻¹ cm⁻¹ in toluene.¹⁰ Yield = 93%. The yield was determined by quantification of the radical concentration by EPR spectroscopy at 23 °C (parameters: frequency = 9.78 GHz, power = 0.2 mW, receiver gain = 5.02×10^4 , mod freq = 100 kHz, mod amp = 0.1 G). The EPR signal ($g = 2.00$) was quantified by double integration and comparison with a TEMPO radical standard calibration curve under non-saturating conditions. The extinction coefficient was calculated using Beer's Law, $\epsilon = A/bc$, where A is the absorbance of the stock solution in toluene at maximum wavelength determined by UV-vis spectroscopy, b is the path length of the UV-vis cuvette (1 cm), and c is the total radical concentration in M.

(*p*-Ph-C₆H₄)₃C•. An amount of tris(*p*-phenylphenyl)methyl bromide (4.94 mM) and excess copper (Cu) powder was added to a scintillation vial in the glove box. Toluene (5 mL) was added to the mixture and was stirred at 75 °C in the dark for 1 h. The dark-purple solution was allowed to cool to 23 °C and then filtered through a Celite[®] plug and used immediately for kinetics experiments. UV-vis (toluene): λ_{max} , nm (ϵ , M⁻¹ cm⁻¹): 565 (580). Radical yield (EPR) = 3.65 mM, 74%. The yield was determined by quantification of the radical concentration by EPR spectroscopy at 23 °C (parameters: frequency = 9.78 GHz, power = 0.2 mW, receiver gain = 5.02×10^4 , mod freq = 100 kHz, mod amp = 0.1 G). The EPR signal ($g = 2.00$) was quantified by double integration and comparison with a TEMPO radical standard calibration curve under non-saturating conditions. The extinction coefficient was calculated using Beer's Law, $\epsilon = A/bc$, where A is the absorbance of the stock solution in toluene at maximum wavelength determined by UV-vis spectroscopy, b is the path length of the UV-vis cuvette (1 cm), and c is the total radical concentration in M.

(*p*-Cl-C₆H₄)₃C•. An amount of tris(*p*-chlorophenyl)methyl bromide (4.69 mM) and excess copper (Cu) powder was added to a scintillation vial in the glove box. Toluene (5 mL) was added to the mixture and was stirred at 75 °C in the dark for 1 h. The red-orange solution was allowed to cool to 23 °C and then filtered through a Celite[®] plug and used immediately for kinetics experiments. UV-vis (toluene): λ_{max} , nm (ϵ , M⁻¹ cm⁻¹): 536 (190). Radical yield (EPR) = 4.52 mM, 96%. The yield was determined by quantification of the radical concentration by EPR spectroscopy at 23 °C (parameters: frequency = 9.78 GHz, power = 0.2 mW, receiver gain = 5.02×10^4 , mod freq = 100 kHz, mod amp = 0.1 G). The EPR signal ($g = 2.00$) was quantified by

double integration and comparison with a TEMPO radical standard calibration curve under non-saturating conditions. The extinction coefficient was calculated using Beer's Law, $\epsilon = A/bc$, where A is the absorbance of the stock solution in toluene at maximum wavelength determined by UV-vis spectroscopy, b is the path length of the UV-vis cuvette (1 cm), and c is the total radical concentration in M.

Reaction of 2 with Gomberg's dimer (Ph_3C)₂. Product analysis. To a solution of **2** in benzene-*d*₆ (5 mM, 500 μL) was added Gomberg's dimer (7.0 mg, 14 μmol , 5.6 equiv) and the internal standard trimethylphenyl silane (TMPS) (11.6 mM). The solution was stirred for 15 min and loaded into an NMR tube. A ¹H NMR spectrum was collected, and the peak from the OH proton of Ph_3COH at 2.28 ppm was integrated versus the peak from the CH_3 groups of trimethylphenylsilane at 0.19 ppm. The reaction was done in triplicate. Average yield_{ROH} = 77%. The same solution in the NMR tube was injected onto the GC-FID, and the Ph_3COH ($R_T = 12.9$ min) product was quantified from a calibration curve with a TMPS ($R_T = 4.2$ min) internal standard. Each reaction was injected twice, and an average yield of 69% was obtained.

Reaction of 2 with (*p*-tBu-C₆H₄)₃C•. Product analysis. To a solution of (*p*-tBu-C₆H₄)₃CBr (6.5 mM, 4 mL) in toluene-*d*₈ was added excess Zn powder (20 mg) and the reaction was stirred in the dark for 3 h at 23 °C. A color change from colorless to yellow was observed, indicating formation of (*p*-tBu-C₆H₄)₃C•. The solution was filtered through Celite® to remove solid Zn, and an aliquot was obtained to determine the concentration by UV-vis spectroscopy. A 500 μL amount of this solution was added to a vial containing solid **2** to make a final mixture of **2** (4.7 mM) and (*p*-tBu-C₆H₄)₃C• (6.4 mM, 1.4 equiv). The internal standard trimethylphenyl silane (TMPS) (11.6 mM) was added, and the solution was stirred for 15 min and loaded into an NMR tube. A ¹H NMR spectrum was collected, and the peak from the t-Bu groups of (*p*-tBu-C₆H₄)₃COH at 1.21 ppm was integrated versus the peak from the CH_3 groups of trimethylphenylsilane at 0.19 ppm. The reaction was done in triplicate. Average yield_{ROH} = 88%. The same solution in the NMR tube was injected to the GC-FID, and the (*p*-tBu-C₆H₄)₃COH ($R_T = 20.7$ min) product was quantified from a calibration curve with a TMPS ($R_T = 4.2$ min) internal standard. Each reaction was injected twice, and an average yield of 89% was obtained.

Incorporation of the ¹⁸O isotope label in Fe^{IV}(¹⁸OH)(tppc) (2-¹⁸O). An amount of crystalline **2** (6 mg, 4.7 μmol) was dissolved in toluene (1 mL) under Ar. An excess amount of H₂¹⁸O (300 μL) was added and the biphasic mixture was stirred vigorously for 3 h until substantial ¹⁸O labeling (70% incorporation) was observed by LDI-MS. The organic layer was then extracted and dried under vacuum with a P₂O₅ trap. The labeled product was used immediately for ¹⁸O product incorporation studies.

Transfer of the ¹⁸O label from Fe^{IV}(¹⁸OH)(tppc) (2-¹⁸O) to trityl radical (Ph_3C)•. In the glove box, to a solution of 2-¹⁸O (70% ¹⁸O) in toluene (9.4 mM, 500 μL) was added Gomberg's dimer (2.3 mg, 1.8 μmol). The solution was stirred for 30 min and then injected directly onto the GC-MS. The intensity of the M⁺ peak corresponding to Ph_3COH ($m/z = 260.1$) was compared to the [M+2]⁺ peak for $\text{Ph}_3\text{C}^{18}\text{OH}$ ($m/z = 262.1$) to determine % incorporation of the ¹⁸O isotope to the trityl alcohol product. A 40% ¹⁸O incorporation was obtained for the alcohol product, which corresponds to a total ¹⁸O incorporation of 57% based on a starting 70% ¹⁸O-labeled **2**. Hydroxyl

exchange of **2** with H₂O is rapid, and the lack of complete ¹⁸O incorporation in the ROH product could be due to back exchange with adventitious H₂O prior to the rebound reaction.

Kinetics studies with Fe^{IV}(OH)(tppc) (2**) and trityl radical derivatives.** In an N₂-filled drybox under low light conditions, the trityl radical derivatives (*p*-X-C₆H₄)₃C• (X = -Cl, -Ph, -tBu, -OMe) were freshly prepared in toluene. Radical concentrations were determined by measuring the UV-vis spectrum and using the known extinction coefficient. Varying amounts of the radical stock solution (50 – 250 μL) were immediately added by syringe to a solution of **2** in toluene (20 μM, 2 mL) to start the reaction. The spectral changes showed isosbestic conversion of **2** (λ_{max} = 405 nm) to **3** (λ_{max} = 420, 575, 765 nm). The pseudo-first-order rate constants, k_{obs}, for these reactions were obtained by using the software Kaleidagraph 4.5 through non-linear least-squares fitting of the plots of absorbance at 570 or 760 nm (Abs_t) versus time (t) according to the equation Abs_t = Abs_f + (Abs₀ – Abs_f) exp(–k_{obs}t), where Abs₀ and Abs_f are the initial and final absorbance, respectively. Second order rate constants (k) were obtained from the slope of the best-fit line from a plot of k_{obs} vs radical concentration.

Preparation of Mössbauer samples. ⁵⁷Fe-enriched complexes **1**, **2** and **3** were used for Mössbauer measurements. Isotopically-labeled samples were synthesized starting from ⁵⁷FeCl₂ (⁵⁷Fe, 95.93%) using the same methods as described for natural abundance FeCl₂. Stock solutions (7.5 mM, 500 μL) were prepared and distributed into custom-made Teflon sample holders, and frozen in liquid N₂ until data collection.

Resonance Raman spectroscopy. Solutions of **1** and **2** in toluene (2 – 5 mM) were prepared in NMR tubes and maintained at 110 K or room temperature during data acquisition. Constant rotation of the NMR tubes was used to minimize the potential for adverse chemistry from the laser irradiation. Comparing consecutive RR spectra with short acquisition time revealed no evidence of photosensitivity for any of the complexes analyzed. Exchange with H/D and ¹⁶O/¹⁸O isotopes on complex **2** was performed directly inside the NMR tube by adding 1 volume of water (D₂O or H₂¹⁸O) to the toluene solution and vigorous mixing for 1 min before collecting RR data on the organic phase. The RR spectra of the corrole complexes were minimally affected by temperature or the addition of water to the toluene solutions, and in all cases the ν(Fe-OH) was observed at 576 cm⁻¹ for the unlabeled complex.

Single crystal X-ray crystallography. All reflection intensities were measured at 110(2) K using a SuperNova diffractometer (equipped with Atlas detector) Cu Kα radiation (λ = 1.54178 Å) under the program CrysAlisPro (Version 1.171.38.43, Rigaku OD, 2015). The same program was used to refine the cell dimensions and for data reduction. The structure was solved with the program SHELXS-2014/7¹¹ and was refined on F² with SHELXL-2014/7¹¹. The temperature of the data collection was controlled using the system Cryojet (manufactured by Oxford Instruments).

Data analysis for Fe^{IV}(Cl)(tppc) (**1**): Analytical numeric absorption correction using a multifaceted crystal model was applied using CrysAlisPro. The H atoms were placed at calculated positions using the instructions AFIX 43 with isotropic displacement parameters having values 1.2 U_{eq} of the attached C atoms. The crystal that was mounted on the diffractometer was not single but two pieces of crystals randomly oriented with each other. The data were integrated as if the crystal was twinned. The two pieces are related by a rotation of ca.

3.52° along the reciprocal vector $0.8559 a^* - 0.4795b^* - 0.1938c^*$ (see .cif file for further details). The BASF scale factor refines to 0.312(15). The crystal lattice contains disordered and/or partially occupied lattice solvent molecules (Et₂O). Their contributions were removed from the final refinement using the SQUEEZE program.¹²

Data analysis for Fe^{IV}(OH)(tppc) (**2**): Empirical absorption correction using spherical harmonics implemented in SCALE3 ABSPACK scaling algorithm was applied using CrysAlisPro. The H atoms were placed at calculated positions (unless otherwise specified) using the instructions AFIX 23, AFIX 43, AFIX 137 or AFIX 147 with isotropic displacement parameters having values 1.2 or 1.5 Ueq of the attached C or O atoms. The position of the hydroxide group is disordered over two sites on opposite sides of the corrole plane. The occupancy factor of the major component of the disorder refines to 0.750(4). The Fe1-O1 bond distance (major component of the disorder) was allowed to refine freely without the use of any geometrical restraints, and this distance refines to 1.857(3) Å based on the experimental data. The Fe1'-O1' bond distance (minor component of the disorder) was restrained using the SAME instruction, to keep the geometry of the minor component consistent with that of the major component. Some phenyl rings from the ligand were also found to be disordered over two orientations. All occupancy factors can be retrieved from the .cif file. The crystal that was mounted on the diffractometer was not a single crystal but rather a composite of 4 different fragments randomly oriented. Each fragment could not be separated as those crystals were fragile and will decompose quickly due to the rapid loss of solvent content. The structure was then refined as a four-component twin (see .cif file for further details), and the BASF scale factors refine to 0.1845(13), 0.0720(15) and 0.0614(18). The crystal lattice also includes disordered pentane lattice solvent molecules. One molecule has been added into the structure model, but the remaining contributions of the other solvent molecules were removed in the final refinement using the SQUEEZE procedure in Platon.¹² The crystallographic data CCDC-1531812-1531813, for **1** and **2** respectively, can be obtained free of charge from the Cambridge Crystallographic Data Centre (www.ccdc.cam.ac.uk/data_request/cif).

Table S1. Crystallographic data for **1**.

Crystal data	
Chemical formula	C ₉₁ H ₅₉ ClFeN ₄
M_r	1299.72
Crystal system, space group	Triclinic, <i>P</i> -1
Temperature (K)	110
a, b, c (Å)	14.2771 (3), 15.7261 (5), 21.1824 (6)
α, β, γ (°)	95.674 (3), 104.611 (2), 109.640 (2)
V (Å ³)	4245.5 (2)
Z	2
Radiation type	Cu $K\alpha$
μ (mm ⁻¹)	2.03
Crystal size (mm)	0.19 × 0.15 × 0.12
Data collection	
Diffractometer	SuperNova, Dual, Cu at zero, Atlas diffractometer
Absorption correction	Analytical <i>CrysAlis PRO</i> , Agilent Technologies, Version 1.171.37.35 (release 13-08-2014 CrysAlis171 .NET) (compiled Aug 13 2014,18:06:01) Analytical numeric absorption correction using a multifaceted crystal model based on expressions derived by R.C. Clark & J.S. Reid. (Clark, R. C. & Reid, J. S. (1995). <i>Acta Cryst. A</i> 51, 887-897) Empirical absorption correction using spherical harmonics, implemented in SCALE3 ABSPACK scaling algorithm.
T_{\min}, T_{\max}	0.737, 0.843
No. of measured, independent and observed [$I > 2\sigma(I)$] reflections	53816, 20239, 12718
R_{int}	0.044
$(\sin \theta/\lambda)_{\text{max}}$ (Å ⁻¹)	0.616
Refinement	
$R[F^2 > 2\sigma(F^2)]$, $wR(F^2)$, S	0.060, 0.169, 0.92
No. of reflections	20239
No. of parameters	875
No. of restraints	48
H-atom treatment	H-atom parameters constrained
$\Delta\rho_{\text{max}}, \Delta\rho_{\text{min}}$ (e Å ⁻³)	2.04, -0.65

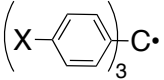
Table S2. Crystallographic data for **2**.

Crystal data	
Chemical formula	C ₉₁ H ₆₀ FeN ₄ O·C ₅ H ₁₂
M_r	1353.42
Crystal system, space group	Triclinic, $P-1$
Temperature (K)	110
a, b, c (Å)	14.1155 (3), 15.7239 (4), 21.2585 (5)
α, β, γ (°)	94.8964 (19), 105.1209 (19), 109.266 (2)
V (Å ³)	4223.12 (18)
Z	2
Radiation type	Cu $K\alpha$
μ (mm ⁻¹)	1.78
Crystal size (mm)	0.18 × 0.16 × 0.14
Data collection	
Diffractometer	SuperNova, Dual, Cu at zero, Atlas
Absorption correction	Multi-scan <i>CrysAlis PRO</i> 1.171.38.43 (Rigaku Oxford Diffraction, 2015) Empirical absorption correction using spherical harmonics, implemented in SCALE3 ABSPACK scaling algorithm.
T_{\min}, T_{\max}	0.054, 1.000
No. of measured, independent and observed [$I > 2\sigma(I)$] reflections	51658, 23950, 13198
R_{int}	0.062
$(\sin \theta/\lambda)_{\text{max}}$ (Å ⁻¹)	0.616
Refinement	
$R[F^2 > 2\sigma(F^2)], wR(F^2), S$	0.057, 0.145, 0.85
No. of reflections	23950
No. of parameters	1154
No. of restraints	777
H-atom treatment	H-atom parameters constrained
$\Delta\rho_{\text{max}}, \Delta\rho_{\text{min}}$ (e Å ⁻³)	0.55, -0.32

Table S3. Selected bond distances (Å) for **1** and **2**.

	1 (X = Cl)	2 (X = O)
Fe1–X1	2.2559(11)	1.857(3)
Fe1–N1	1.872(3)	1.876(3)
Fe1–N2	1.895(3)	1.902(3)
Fe1–N3	1.904(2)	1.905(3)
Fe1–N4	1.880(3)	1.882(3)
Fe1–(N _{pyrrole}) _{plane}	0.341	0.383
Fe1–(23-atom) _{plane}	0.329	0.352
C _β –C _β (av)	1.370(4)	1.366(4)
C _α –C _β (av)	1.428(4)	1.427(4)
C _α –C _α (C1–C19)	1.407(4)	1.429(4)
C _α –N _{pyrrole} (av)	1.382(4)	1.377(4)
C _α –C _{meso} (av)	1.404(4)	1.399(4)

Table S4. Redox potentials, Hammett parameters, and second order rate constants for the reaction of **2** with the *para*-substituted trityl radical derivatives used in the study.

	E _{1/2} , (V vs Fc ⁺⁰) ^a	3σ ⁺ _{para} ^b	k (M ⁻¹ s ⁻¹)
-OMe	-0.58	-2.33	357(4)
-tBu	-0.25	-0.77	49(1)
-Ph	-0.19	-0.54	31(2)
-Cl	0.00	+0.34	12.6(1)

^a For the reaction: Ar₃C⁺ + e⁻ → Ar₃C• in CH₃CN at 25 °C, Ref 13.^b Ref 14.

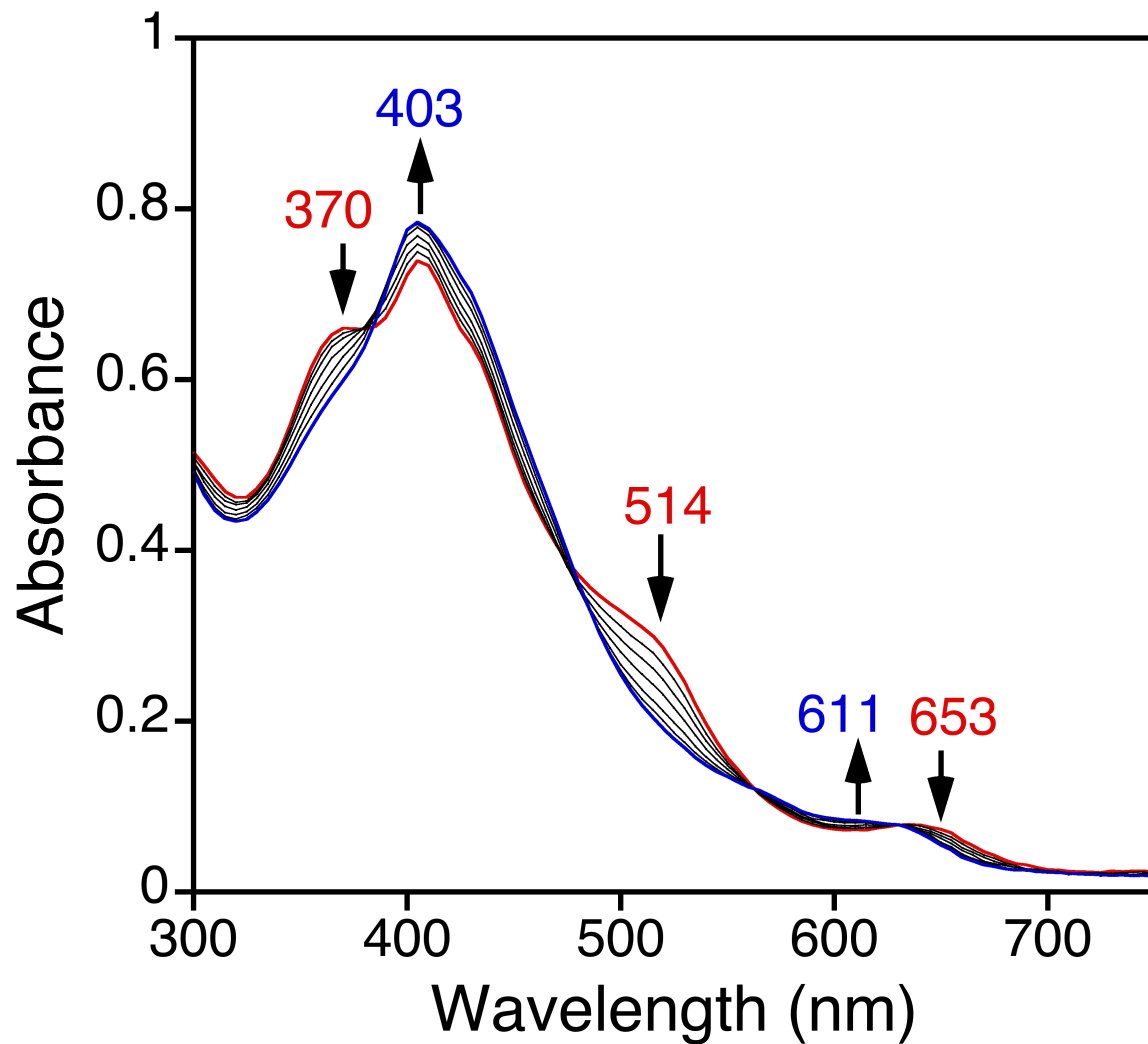


Fig. S1. UV-vis spectral titration of $\text{Fe}^{\text{IV}}(\text{Cl})(\text{tppc})$ (**1**, red line) (20 μM , in toluene) with $\text{Bu}_4\text{N}^+\text{OH}^-$ (0-1 equiv, in CH_3CN) to form $\text{Fe}^{\text{IV}}(\text{OH})(\text{tppc})$ (**2**, blue line) at 23 $^\circ\text{C}$.

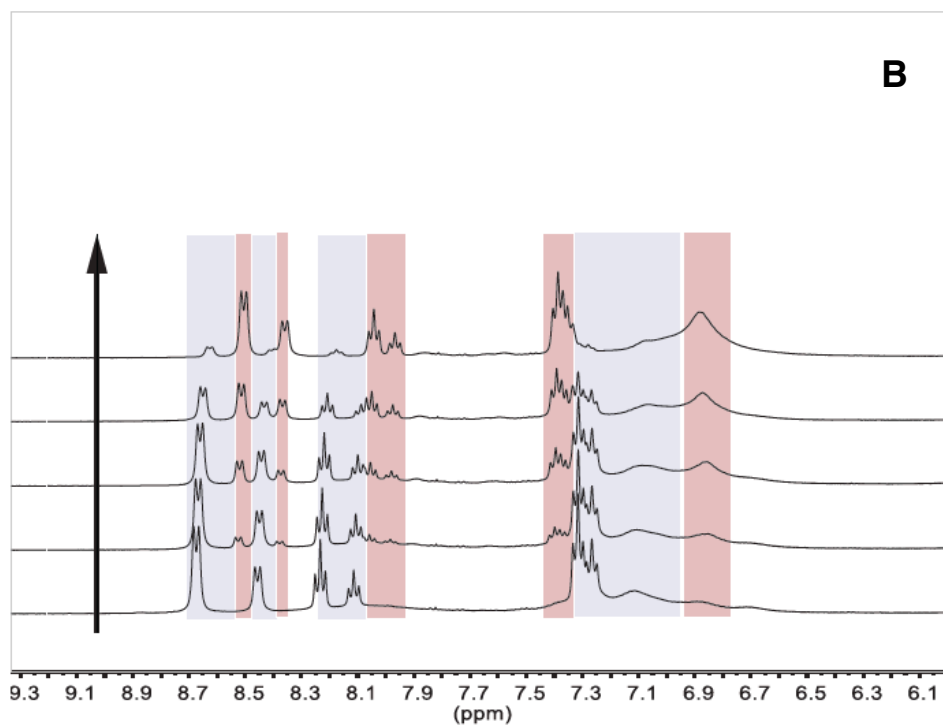
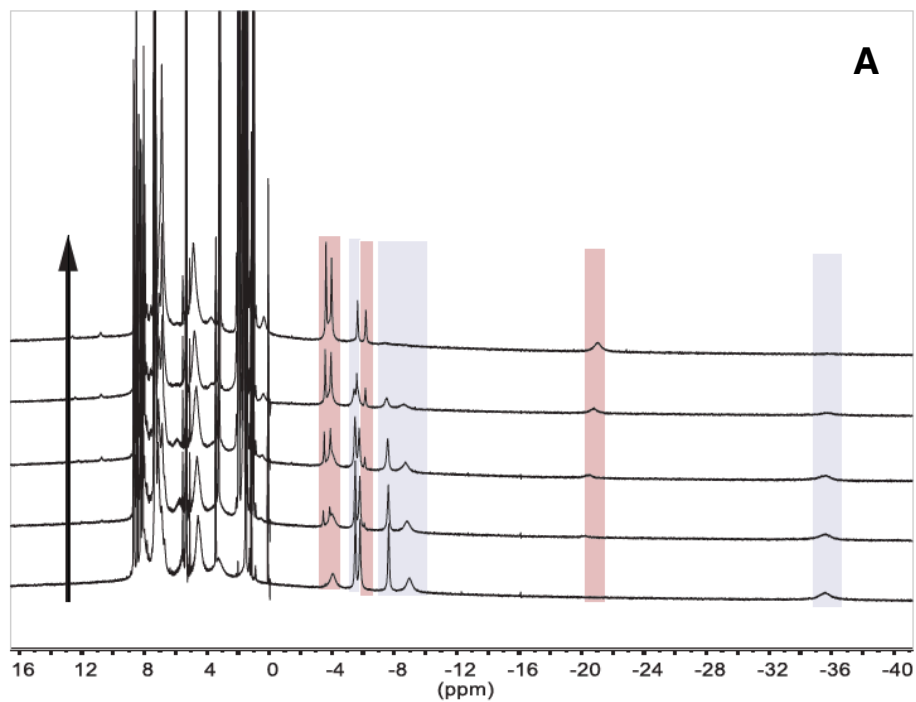


Fig. S2. ^1H NMR titration of $\text{Fe}^{\text{IV}}(\text{Cl})(\text{tppc})$ (**1**, bottom spectrum) (4 mM, in $\text{toluene-}d_8$) with $\text{Bu}_4\text{N}^+\text{OH}^-$ (0 – 1 equiv, in CD_3CN) in 0.25 equiv increments to form $\text{Fe}^{\text{IV}}(\text{OH})(\text{tppc})$ (**2**, top spectrum) at 23 °C. a) entire spectral region, b) aromatic region. The purple highlight shows the disappearing peaks from **1** and the red highlight shows the growing peaks from **2**.

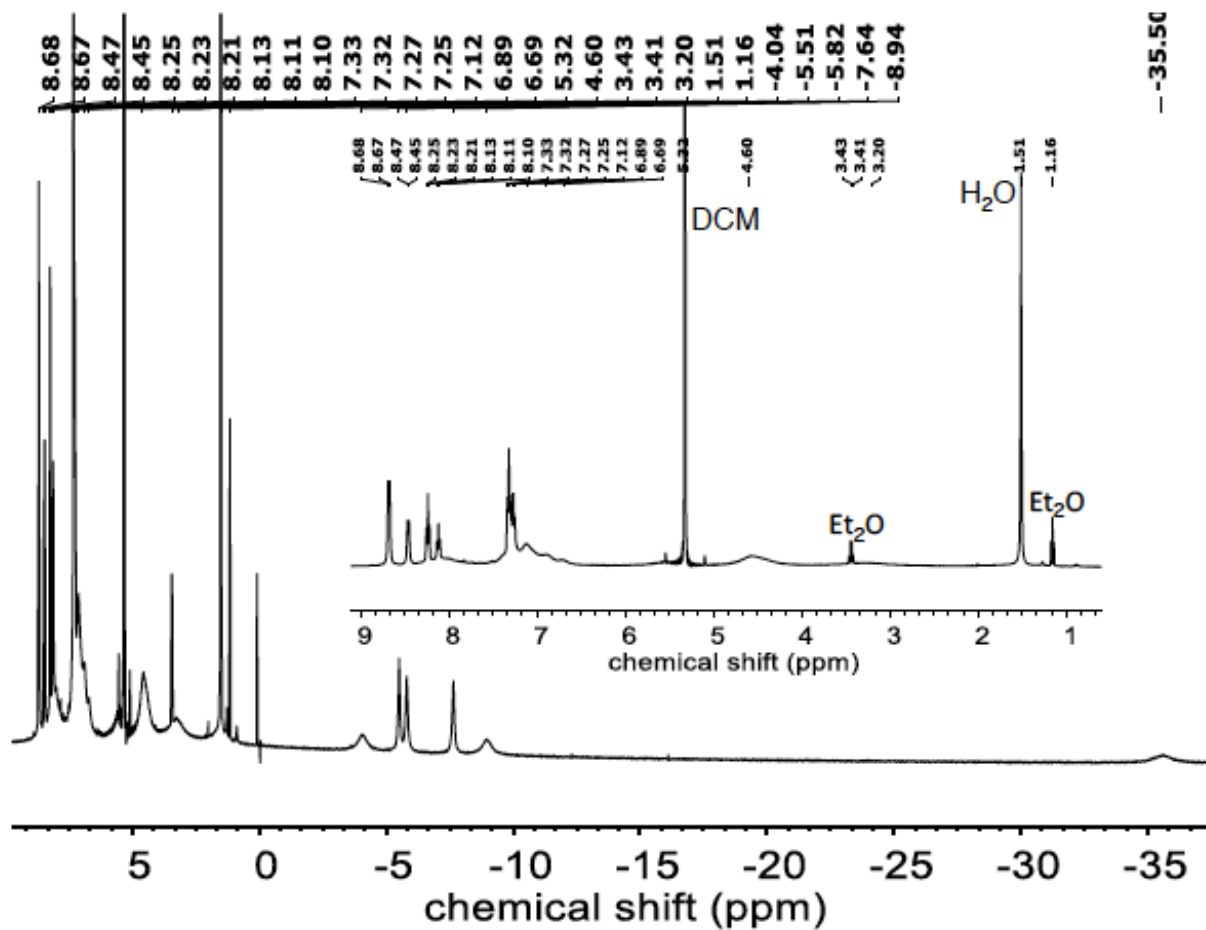


Fig. S3. ¹H NMR spectrum (400 MHz) of crystalline Fe^{IV}(Cl)(tppc) (**1**) in CD₂Cl₂ at 23 °C. Inset: spectrum showing region from 1 – 9 ppm.

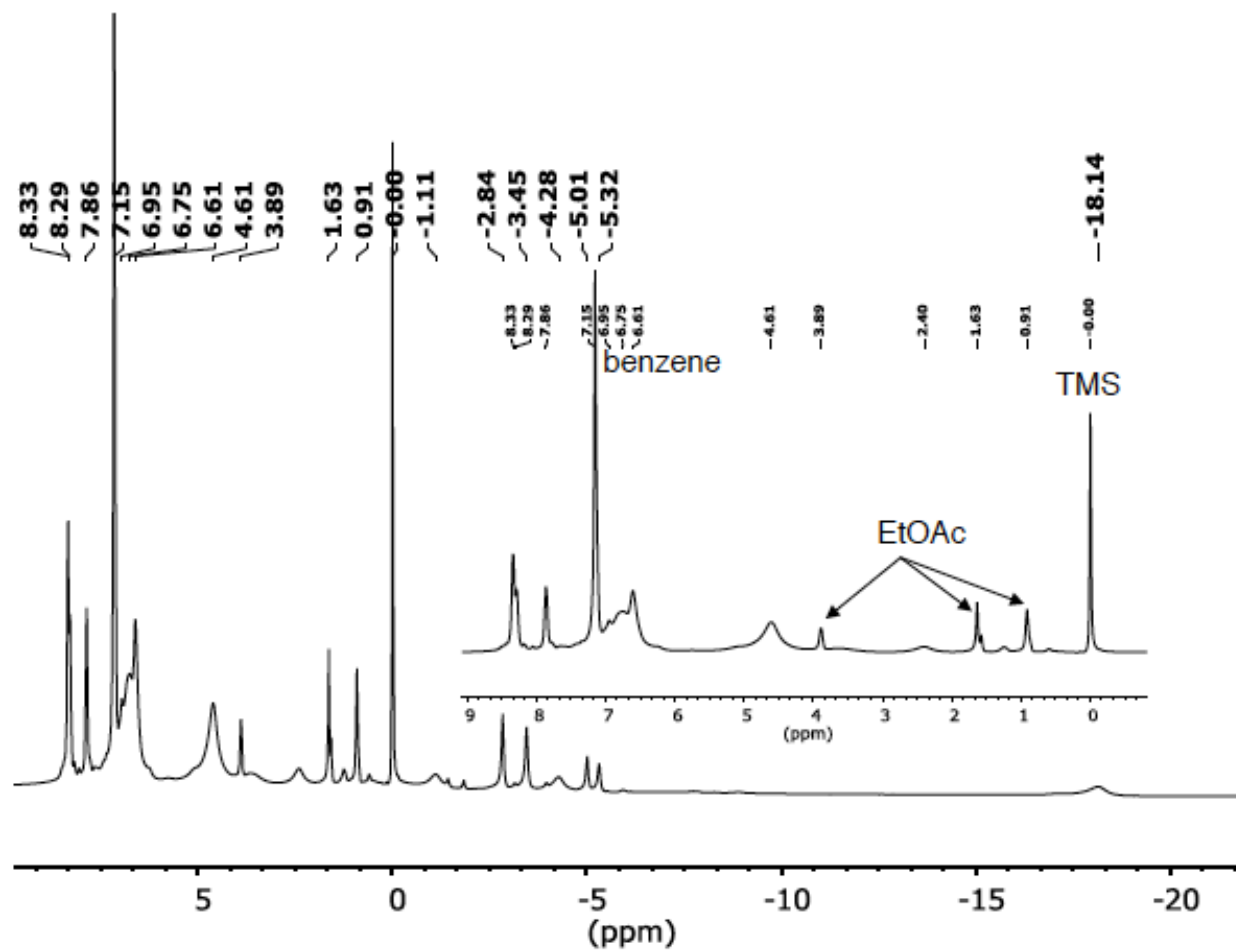


Fig. S4. ^1H NMR spectrum (400 MHz) of crystalline $\text{Fe}^{\text{IV}}(\text{OH})(\text{tppc})$ (**2**) in C_6D_6 at 23°C . Inset: spectrum showing region from 0 – 9 ppm.

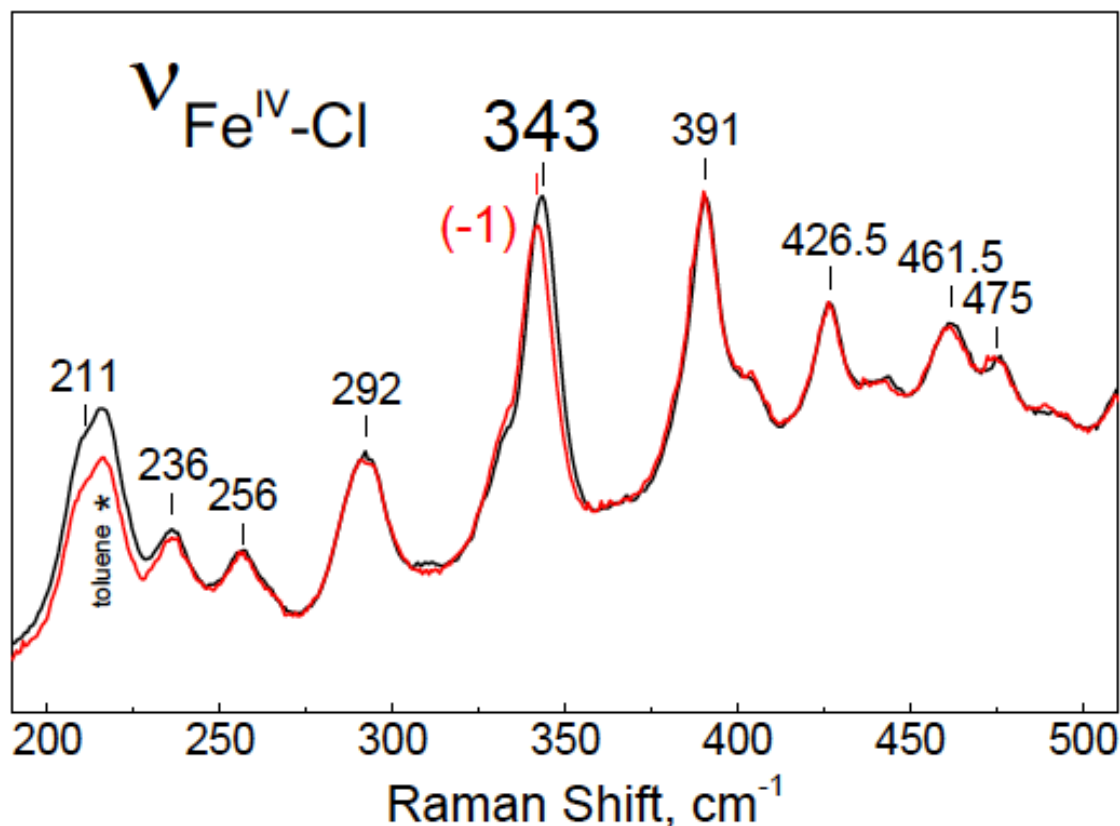


Fig. S5. Resonance Raman spectra of **1** (black line) and ^{57}Fe -labeled **1** (red line). The 343-cm^{-1} band is assigned to the $\nu(\text{Fe}^{\text{IV}}\text{-Cl})$ mode on the basis of comparable stretching frequencies in terminal Fe-Cl complexes¹⁵ and $\text{Fe}^{\text{III}}(\text{Cl})$ porphyrins ($\nu(\text{Fe-Cl}) = 359\text{-}379\text{ cm}^{-1}$),¹⁶ and on the disappearance of this band in the RR spectra of **2**; the assignment is confirmed by the 1-cm^{-1} downshift observed with ^{57}Fe labeling; this -1 cm^{-1} shift matches the calculated value based on Hooke's law for a ^{57}Fe substitution in an isolated Fe-Cl diatomic oscillator: $\nu(^{57}\text{Fe}^{\text{IV}}\text{-Cl}) = 342\text{ cm}^{-1}$.

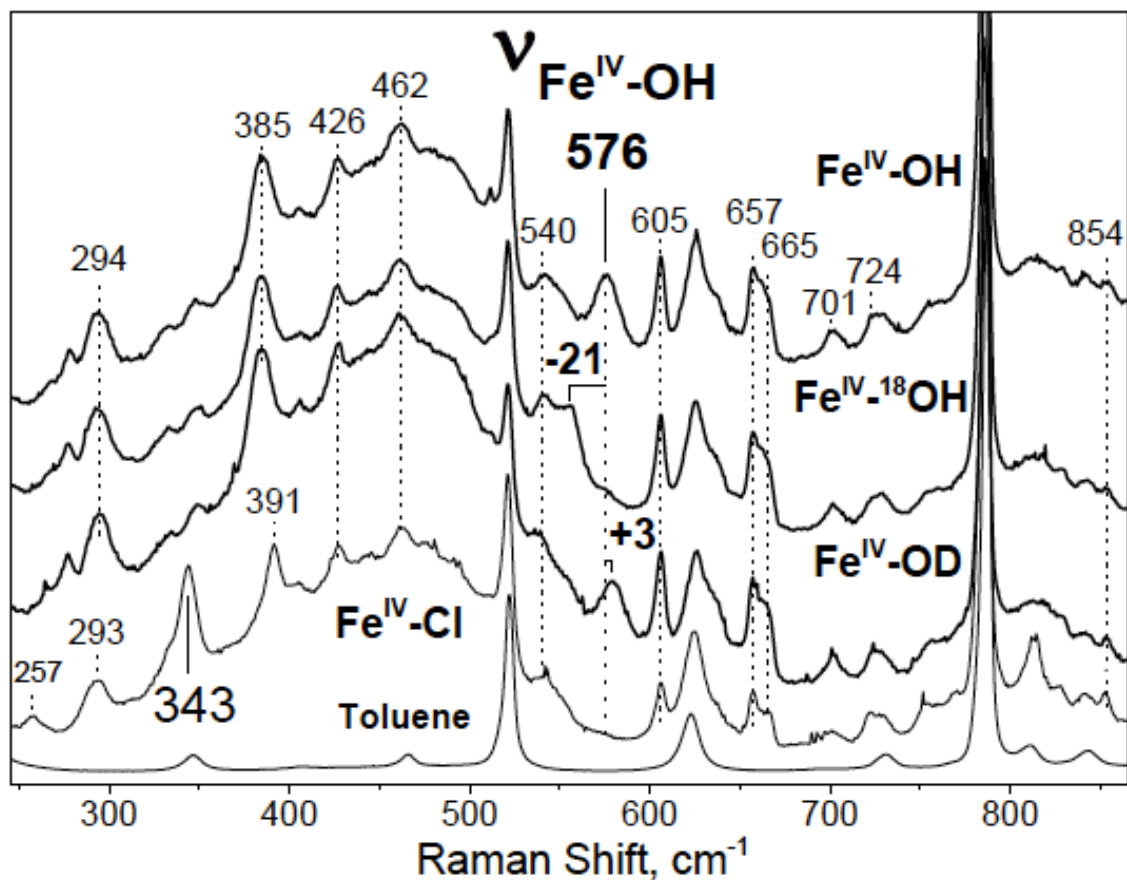


Fig. S6. Resonance Raman spectra of (from top to bottom): **2**, ^{18}O -labeled **2**, D-labeled **2**, **1**, and toluene blank. Experimental and calculated isotopic shifts: $\nu(\text{Fe-}^{18}\text{OH}) = 555$ (calc. 551) cm^{-1} ($\Delta\nu(\text{Fe-OH}) = -21$ (calc. -25)), $\nu(\text{Fe}^{\text{IV}}\text{-OD}) = 579$ (calc. 563) cm^{-1} ($\Delta\nu(\text{Fe-OH}) = +3$ (calc. -13)). Upon mixing **2** with D_2O , the peak at 576 cm^{-1} shifts by $+3$ cm^{-1} , in contrast to the expected -13 cm^{-1} downshift for an Fe-(OD) oscillator. This upshift might be due to a weaker hydrogen bonding between an Fe-OD (as opposed to Fe-OH) group and a water molecule.

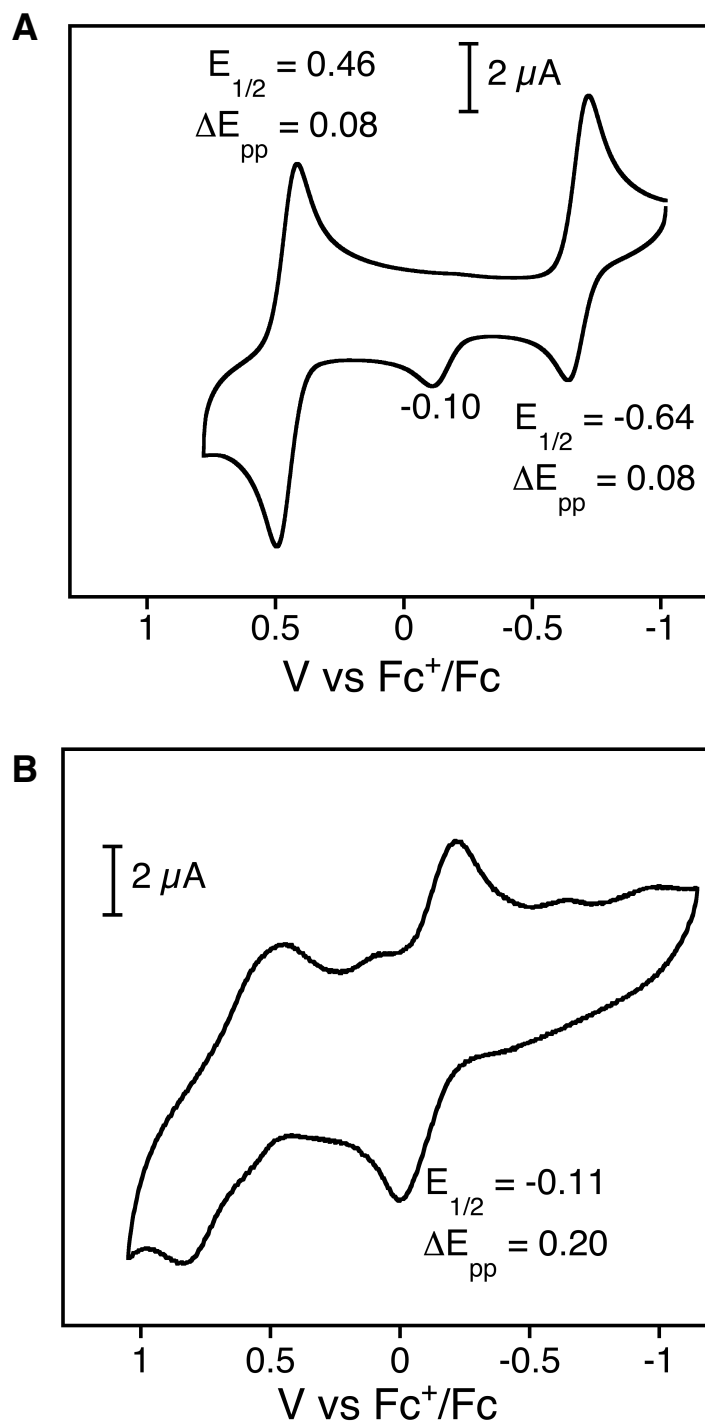


Fig. S7. Cyclic voltammogram of A) **1** in CH_2Cl_2 and B) **2** in benzonitrile. The solutions of complex (0.5 mM) contain $Bu_4N^+PF_6^-$ (0.1 M) supporting electrolyte, with a 100 mV/s scan rate. The redox potentials were referenced versus a ferrocene external standard.

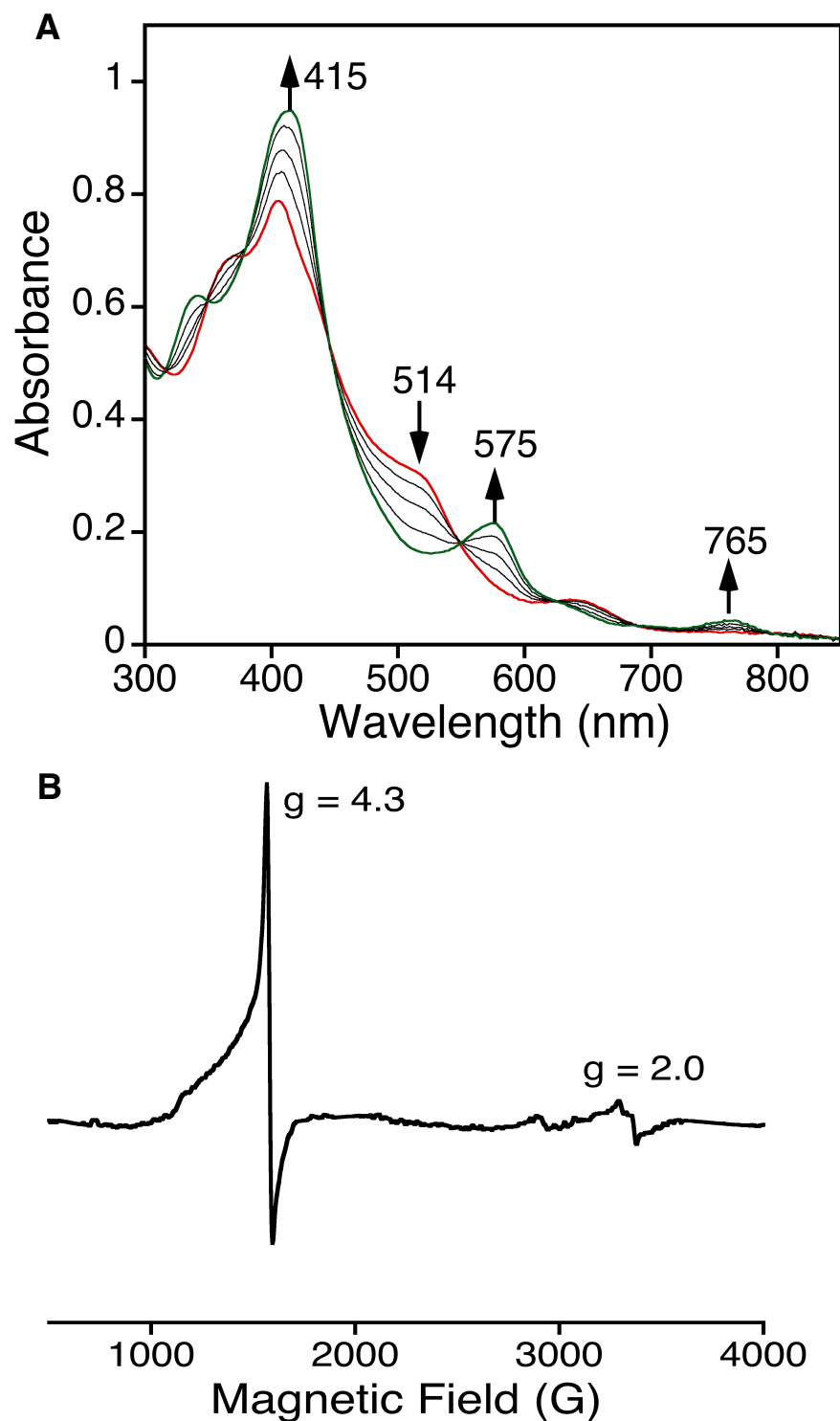


Fig. S8. a) UV-vis spectral titration of Fe^{IV}(Cl)(tppc) (**1**, red line) (20 μ M) with Cr(C₆H₆)₂ (0 – 1 equiv) in CH₂Cl₂ at 23 °C to form Fe^{III}(tppc) (**3**, green line). b) X-band EPR spectrum of Fe^{III}(tppc) (**3**) in toluene, sample conc. = 2 mM, parameters: T= 16 K, freq. = 9.427 GHz, power = 0.20 mW, mod. amp. = 10 G, mod. freq. = 100 kHz, receiver gain = 5.02 $\times 10^3$, NS = 2.

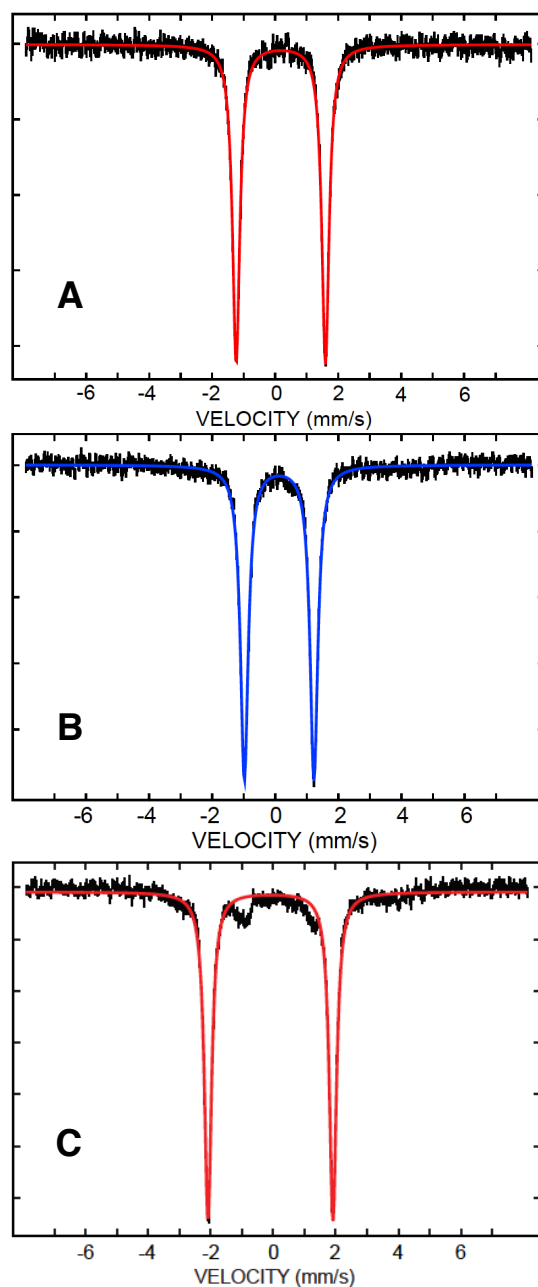


Fig. S9. Mössbauer spectra of a) $\text{Fe}^{\text{IV}}(\text{Cl})(\text{tppc})$ (**1**), b) $\text{Fe}^{\text{IV}}(\text{OH})(\text{tppc})$ (**2**), c) $\text{Fe}^{\text{III}}(\text{OEt}_2)_2(\text{tppc})$ (**3**) in toluene at 4.2 K. Mössbauer parameters, **1**: $\delta = 0.18$ mm/s, $\Delta E_{\text{Q}} = 2.86$ mm/s, **2**: $\delta = 0.13$ mm/s, $\Delta E_{\text{Q}} = 2.21$ mm/s, **3**: $\delta = -0.09$ mm/s, $\Delta E_{\text{Q}} = 4.00$ mm/s.

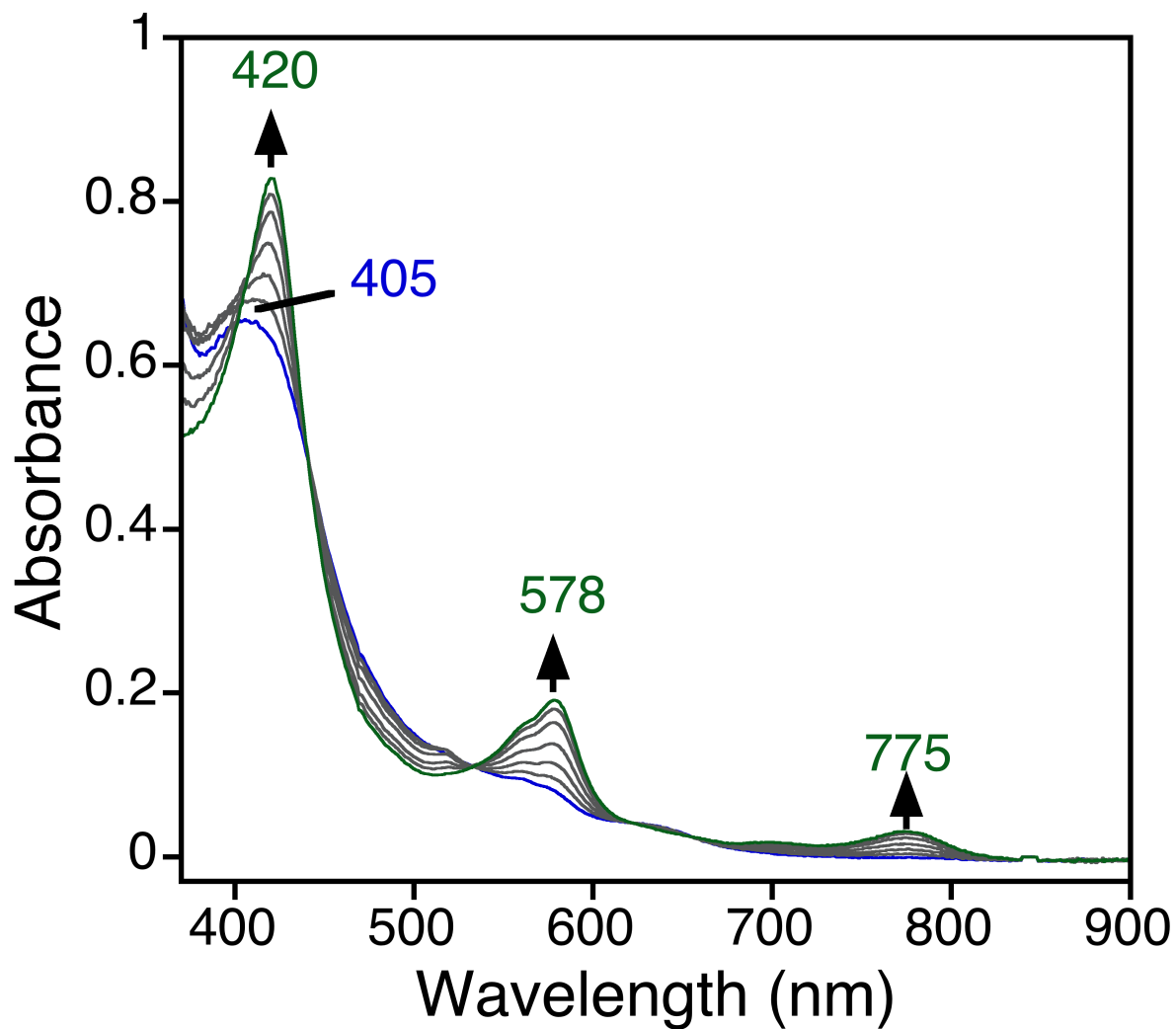


Fig. S10. Time-resolved UV-vis spectral changes (0 – 50 s) for the reaction of **2** (blue line, 20 μM) and Gomberg's dimer $(\text{Ph}_3\text{C})_2$ (110 equiv) in toluene at 23 $^\circ\text{C}$ to form **3** (green line).

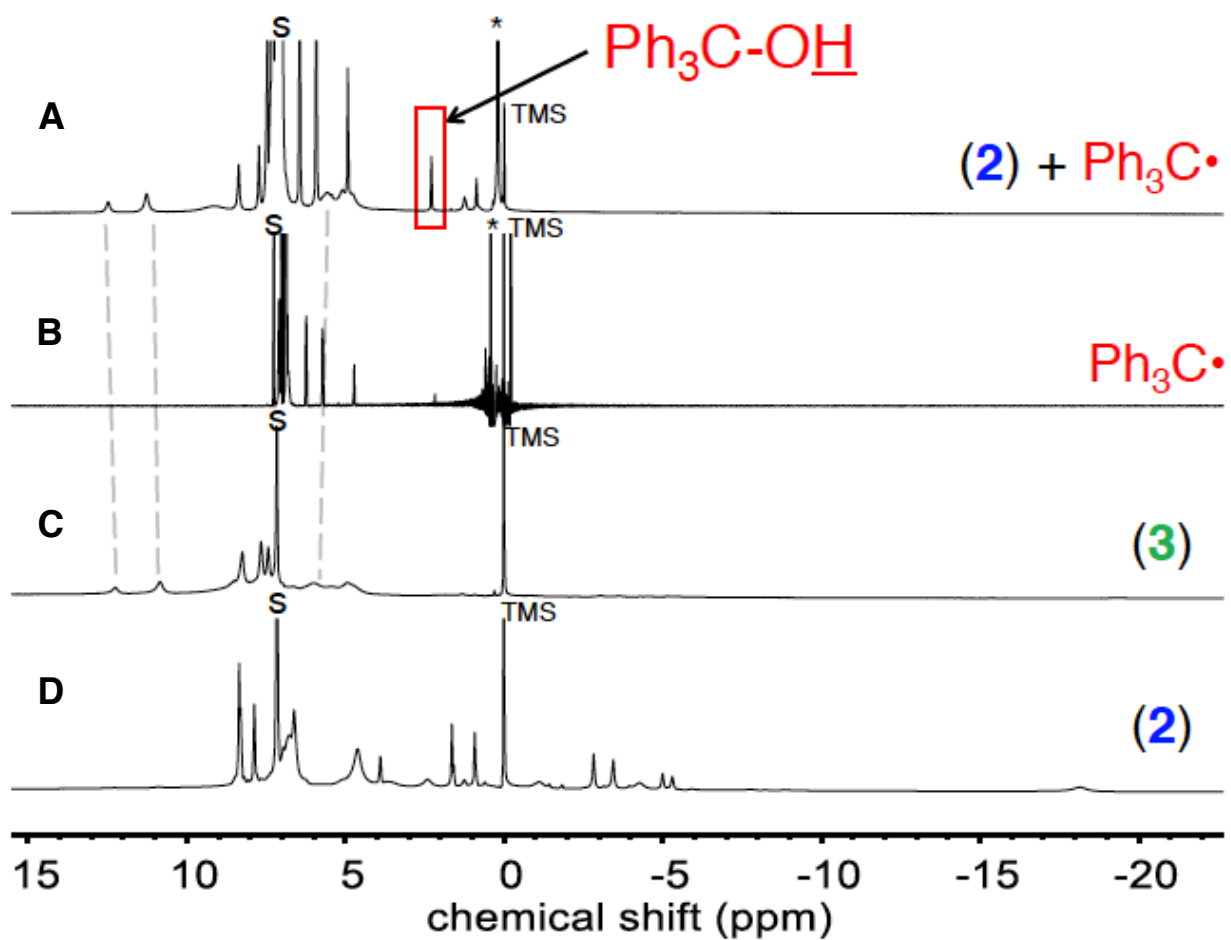


Fig. S11. ^1H NMR spectra for a) the reaction of **2** (5 mM) with Gomberg's dimer (Ph_3C)₂ (5.6 equiv) in benzene- d_6 to form Ph_3COH (boxed in red) and **3**, b) Gomberg's dimer in benzene- d_6 , c) **3** in benzene- d_6 , and d) **2** in benzene- d_6 . s = solvent (benzene) peak, * = trimethylphenylsilane internal standard, TMS = tetramethylsilane reference.

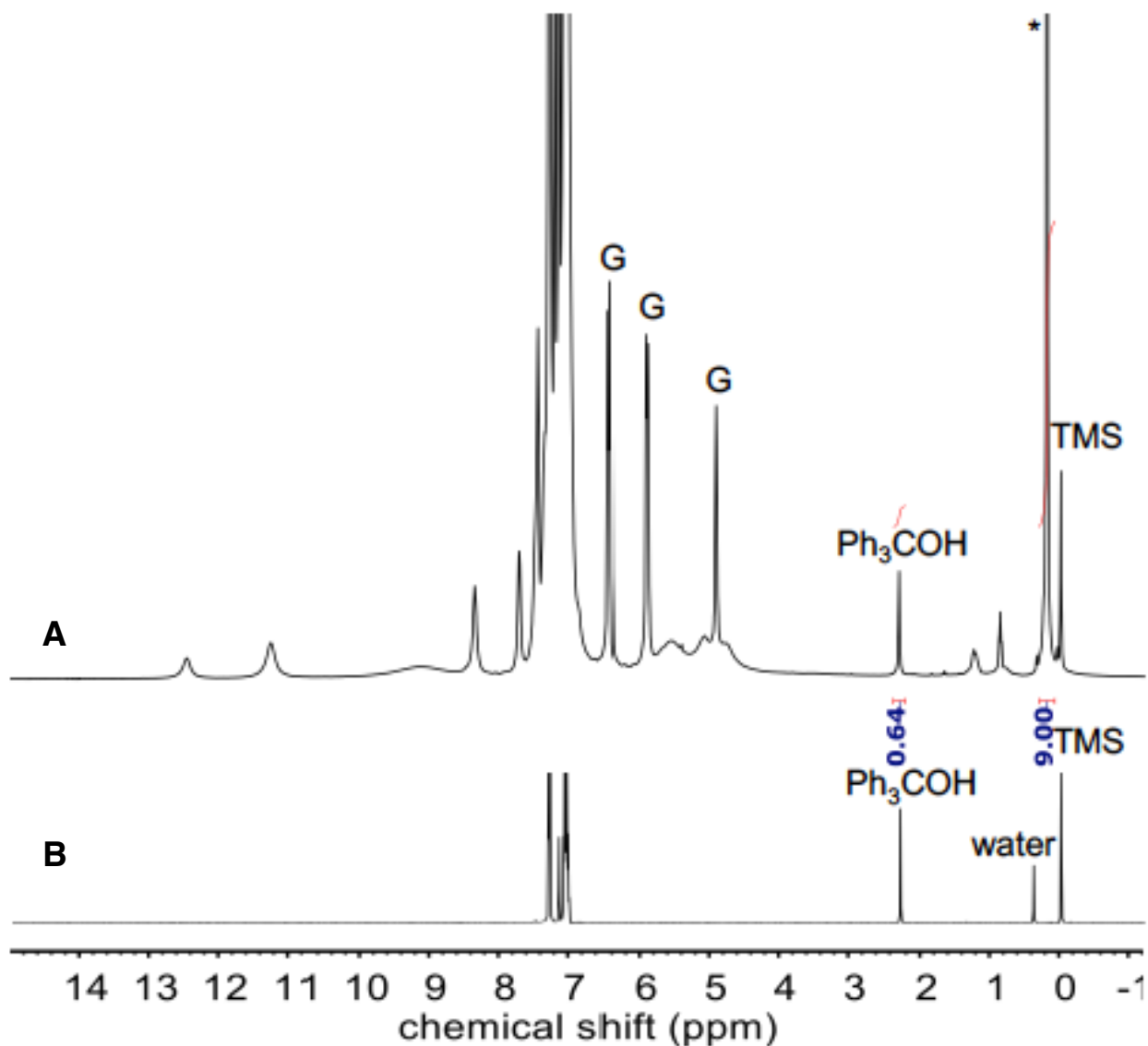


Fig. S12. ^1H NMR spectra for a) the reaction of **2** (5 mM) with Gomberg's dimer (Ph_3C)₂ (5.6 equiv) in benzene- d_6 to form Ph_3COH . The peak from the OH proton of Ph_3COH at 2.28 ppm was integrated versus the peak from the CH_3 groups of trimethylphenylsilane at 0.19 ppm. $\text{Yield}_{\text{ROH}} = 77\%$. s = solvent (benzene) peak, * = trimethylphenylsilane internal standard, TMS = tetramethylsilane reference, G = unreacted Gomberg's dimer b) triphenylmethanol in benzene- d_6 . Labeled peak corresponds to the OH proton of Ph_3COH at 2.28 ppm.

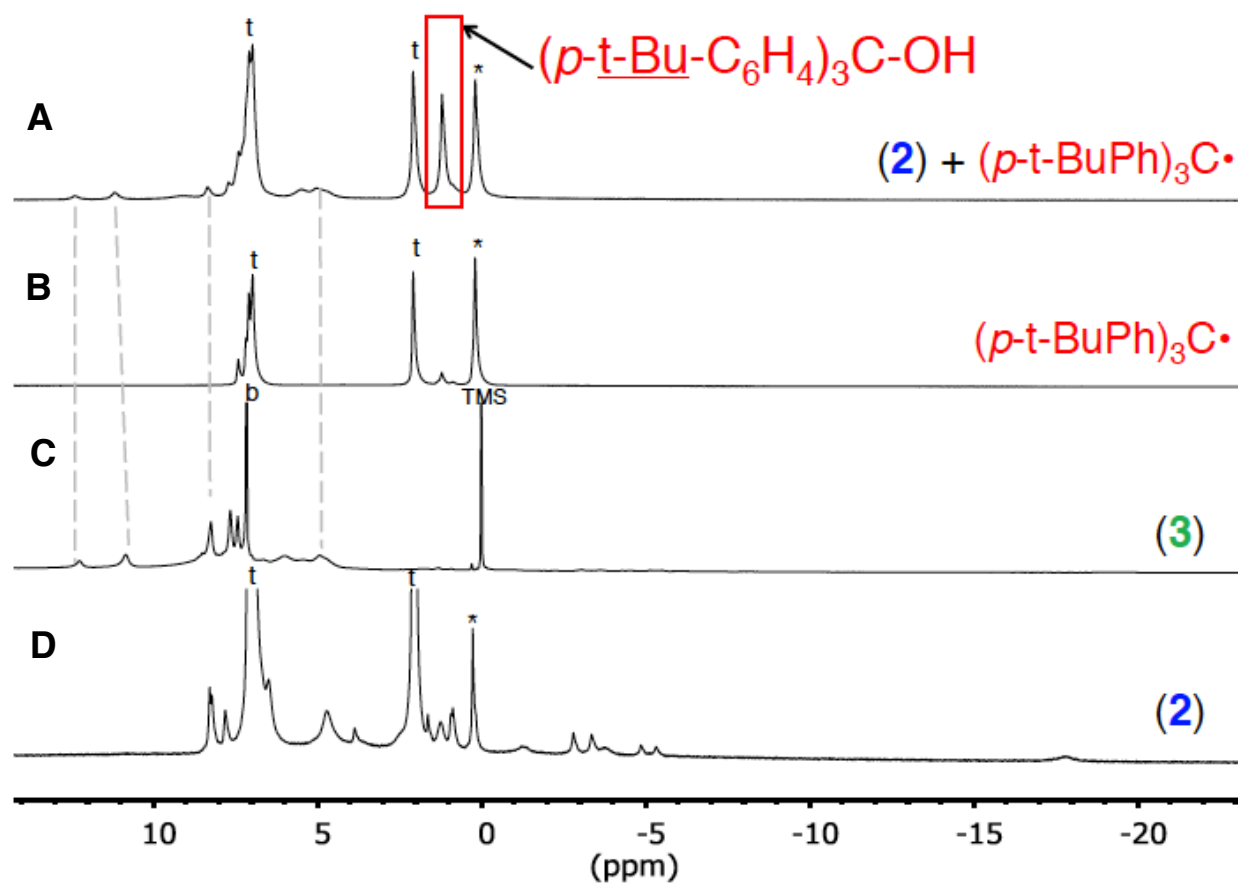


Fig. S13. ^1H NMR spectra for a) the reaction of **2** (4.7 mM) with $(p\text{-t-Bu-C}_6\text{H}_4)_3\text{C}\cdot$ (1.4 equiv) in toluene- d_8 to form $(p\text{-t-Bu-C}_6\text{H}_4)_3\text{COH}$ (boxed in red) and **3** b) $(p\text{-t-Bu-C}_6\text{H}_4)_3\text{C}\cdot$ in toluene- d_8 , c) **3** in benzene- d_6 , and d) **2** in toluene- d_8 . * = trimethylphenylsilane internal standard, TMS = tetramethylsilane reference, t = toluene solvent peaks, b = benzene solvent peak.

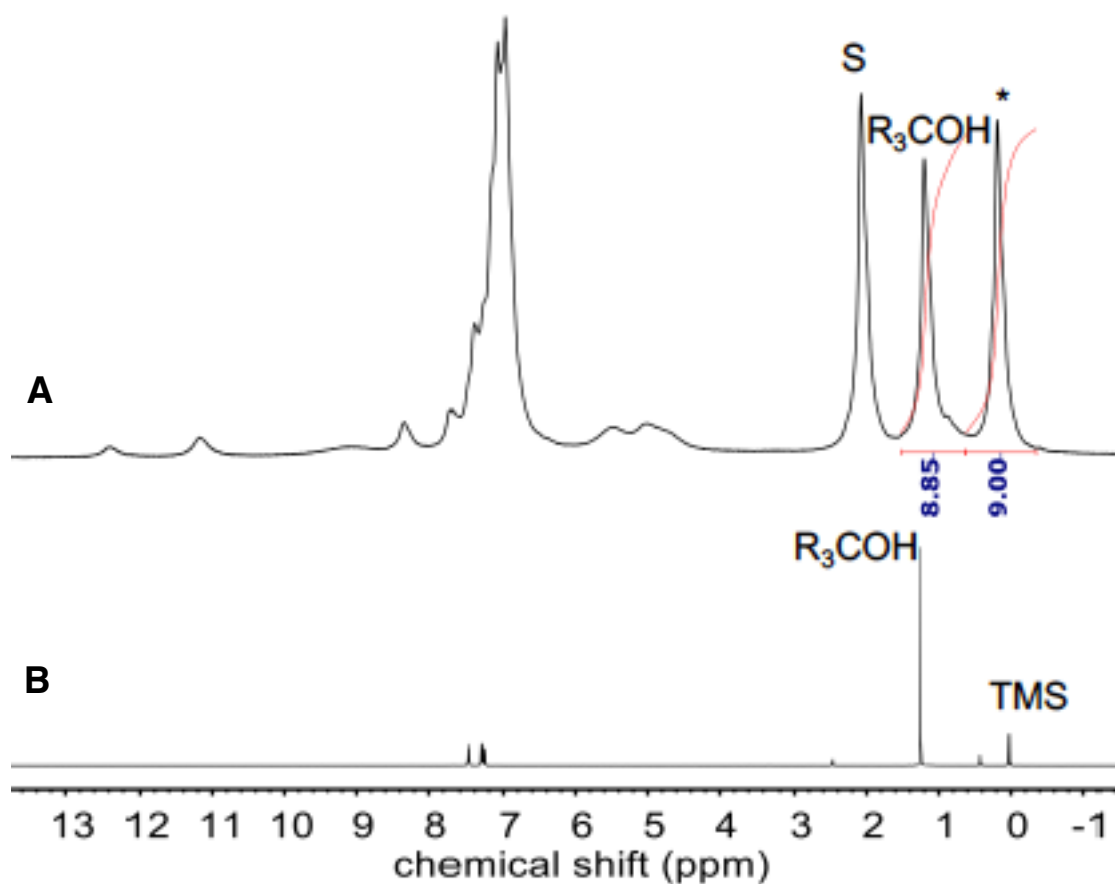


Fig. S14. ¹H NMR spectra for a) the reaction of **2** (4.7 mM) with (*p*-t-Bu-C₆H₄)₃C• (1.4 equiv) in toluene-*d*₈ to form (*p*-t-Bu-C₆H₄)₃COH. The peak from the t-Bu groups of (*p*-t-Bu-C₆H₄)₃COH at 1.21 ppm was integrated versus the peak from the CH₃ groups of trimethylphenylsilane at 0.19 ppm. Yield_{ROH} = 88%. s = solvent (toluene) peaks, * = trimethylphenylsilane internal standard b) (*p*-t-Bu-C₆H₄)₃COH in toluene-*d*₈. Labeled peak corresponds to the t-Bu group of (*p*-t-Bu-C₆H₄)₃COH at 1.21 ppm.

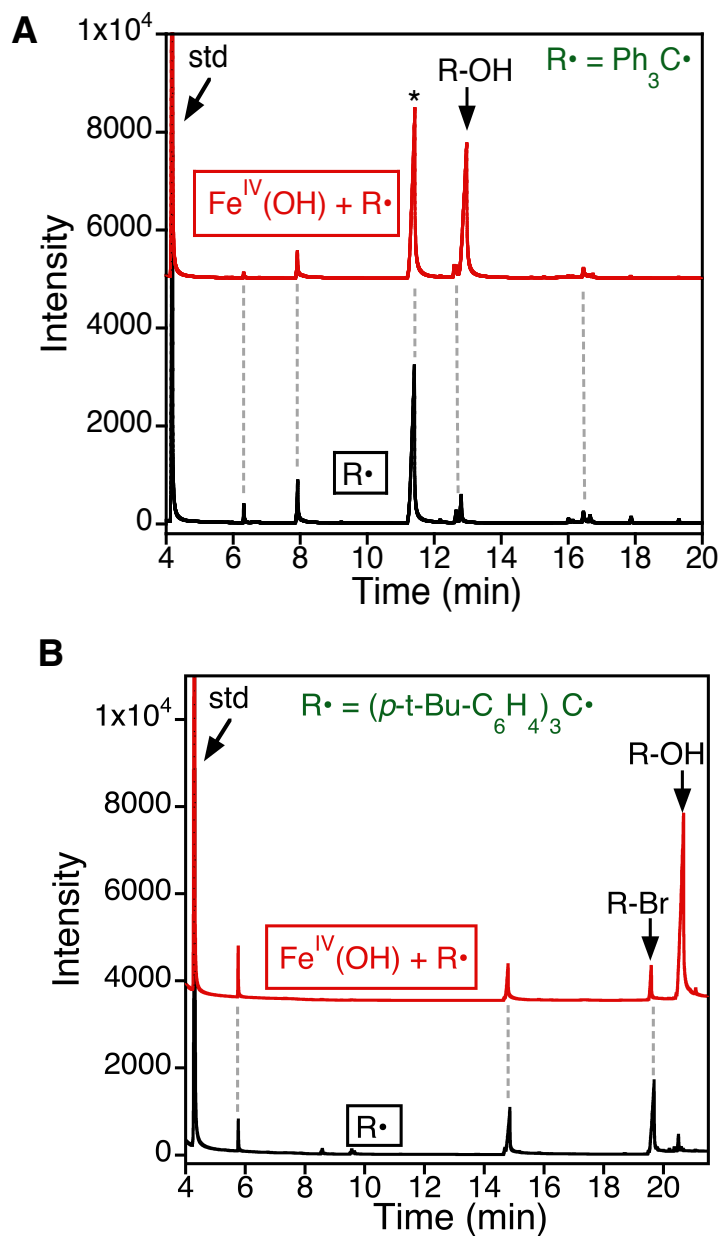


Fig. S15. GC traces for a) the reaction of **2** (5 mM) with Gomberg's dimer (5.6 equiv) (red trace) and Gomberg's dimer alone (black). The Ph_3COH peak ($R_t = 12.9$ min) was quantified against an internal standard, trimethylphenylsilane ($R_t = 4.2$ min), $\text{yield}_{\text{ROH}} = 69\%$. The unlabeled peaks are unidentified decomposition products, which were also present in the GC trace of Gomberg's dimer alone (shown by the grey dotted lines). b) the reaction of **2** (4.7 mM) with $(p\text{-}t\text{-Bu-C}_6\text{H}_4)_3\text{C}\cdot$ (1.4 equiv) and $(p\text{-}t\text{-Bu-C}_6\text{H}_4)_3\text{C}\cdot$ alone (black). The $(p\text{-}t\text{-Bu-C}_6\text{H}_4)_3\text{COH}$ peak ($R_t = 20.7$ min) was quantified against an internal standard, trimethylphenylsilane ($R_t = 4.2$ min), $\text{yield}_{\text{ROH}} = 89\%$. Unreacted starting material $(p\text{-}t\text{-Bu-C}_6\text{H}_4)_3\text{CBr}$ ($R_t = 19.7$ min) was also observed. The unlabeled peaks are unidentified decomposition products, which were also present in the GC trace of $(p\text{-}t\text{-Bu-C}_6\text{H}_4)_3\text{C}\cdot$ alone (shown by the grey dotted lines).

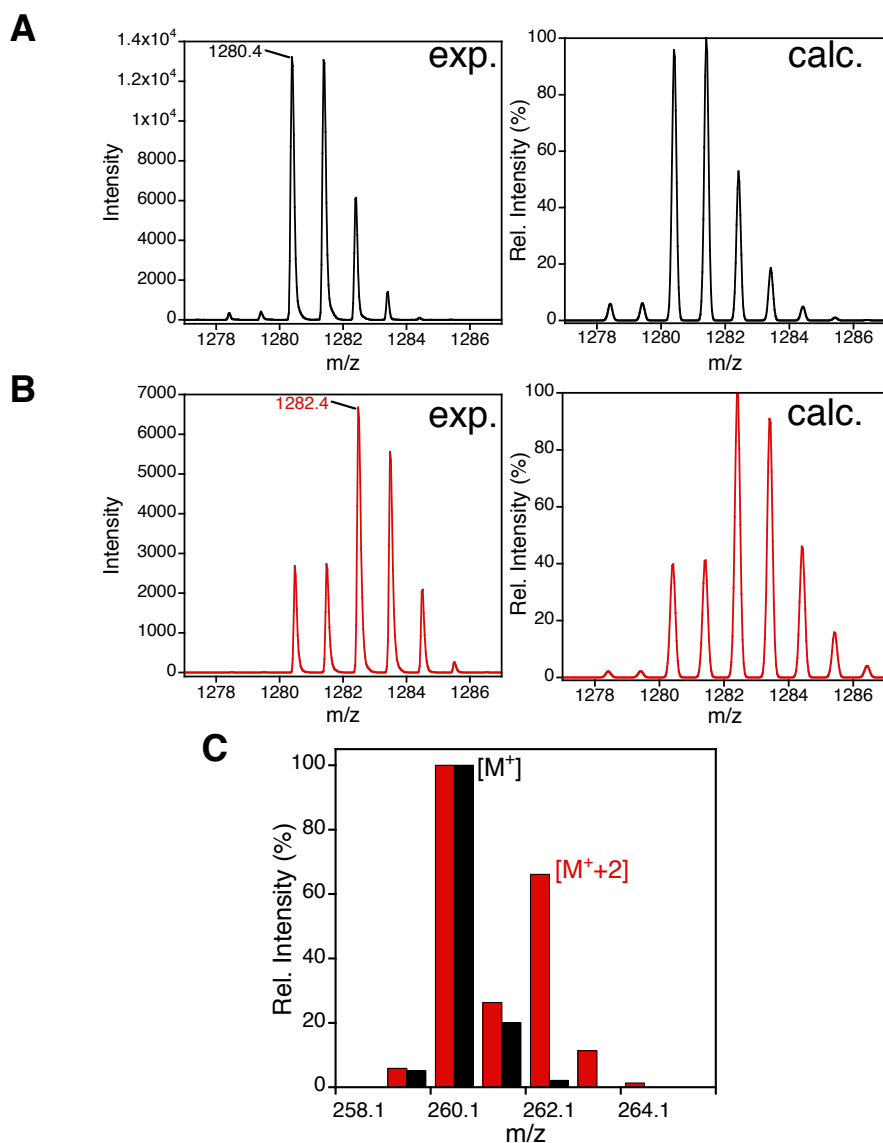


Fig. S16. Experimental and calculated LDI-MS of a) $\text{Fe}^{\text{IV}}(^{16}\text{OH})(\text{tppc})$, b) $\text{Fe}^{\text{IV}}(^{18}\text{OH})(\text{tppc})$ (70% ^{18}O incorporation) and c) EI-MS of the Ph_3COH peak after reaction with ^{18}O labeled (red, 40% ^{18}O incorporation) and unlabeled (black) $\text{Fe}^{\text{IV}}(\text{OH})(\text{tppc})$. Total ^{18}O incorporation: (40% ^{18}O incorporation in product) / (70% ^{18}O -labeled starting material **2**) = 57%.

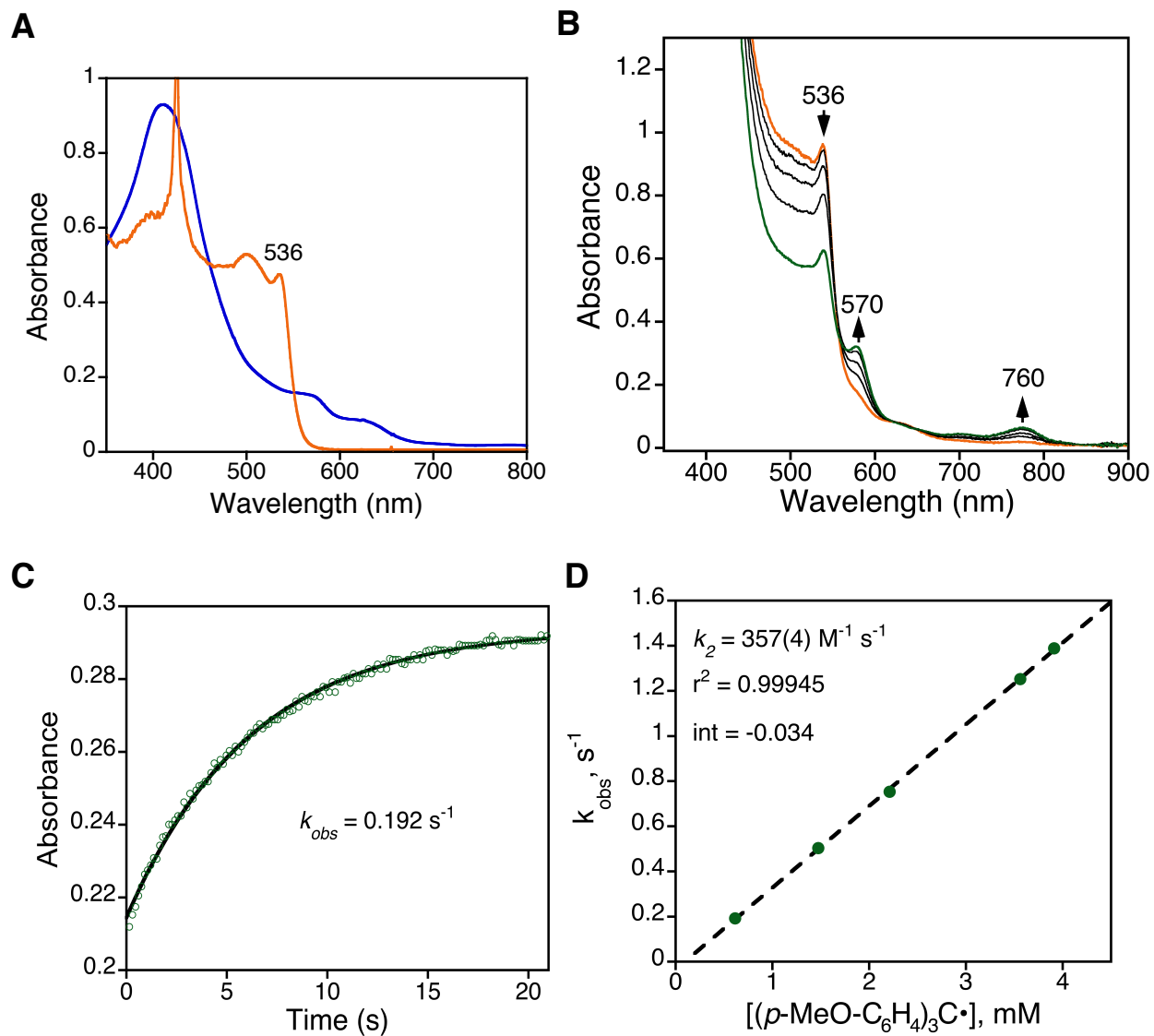


Fig. S17. a) Overlay of UV-vis spectra of **2** (blue) and $(p\text{-MeO-C}_6\text{H}_4)_3\text{C}\cdot$ (orange). b) Time-resolved UV-vis spectral changes for the reaction of **2** (20 μM) and $(p\text{-MeO-C}_6\text{H}_4)_3\text{C}\cdot$ (1.43 mM) in toluene at 23 $^\circ\text{C}$ (orange line, $t = 0.15$ s) to form **3** (green line, $t = 20$ s). c) Changes in absorbance vs time for the growth of **3** (570 nm) (green circles). d) Plot of k_{obs} versus $[(p\text{-MeO-C}_6\text{H}_4)_3\text{C}\cdot]$.

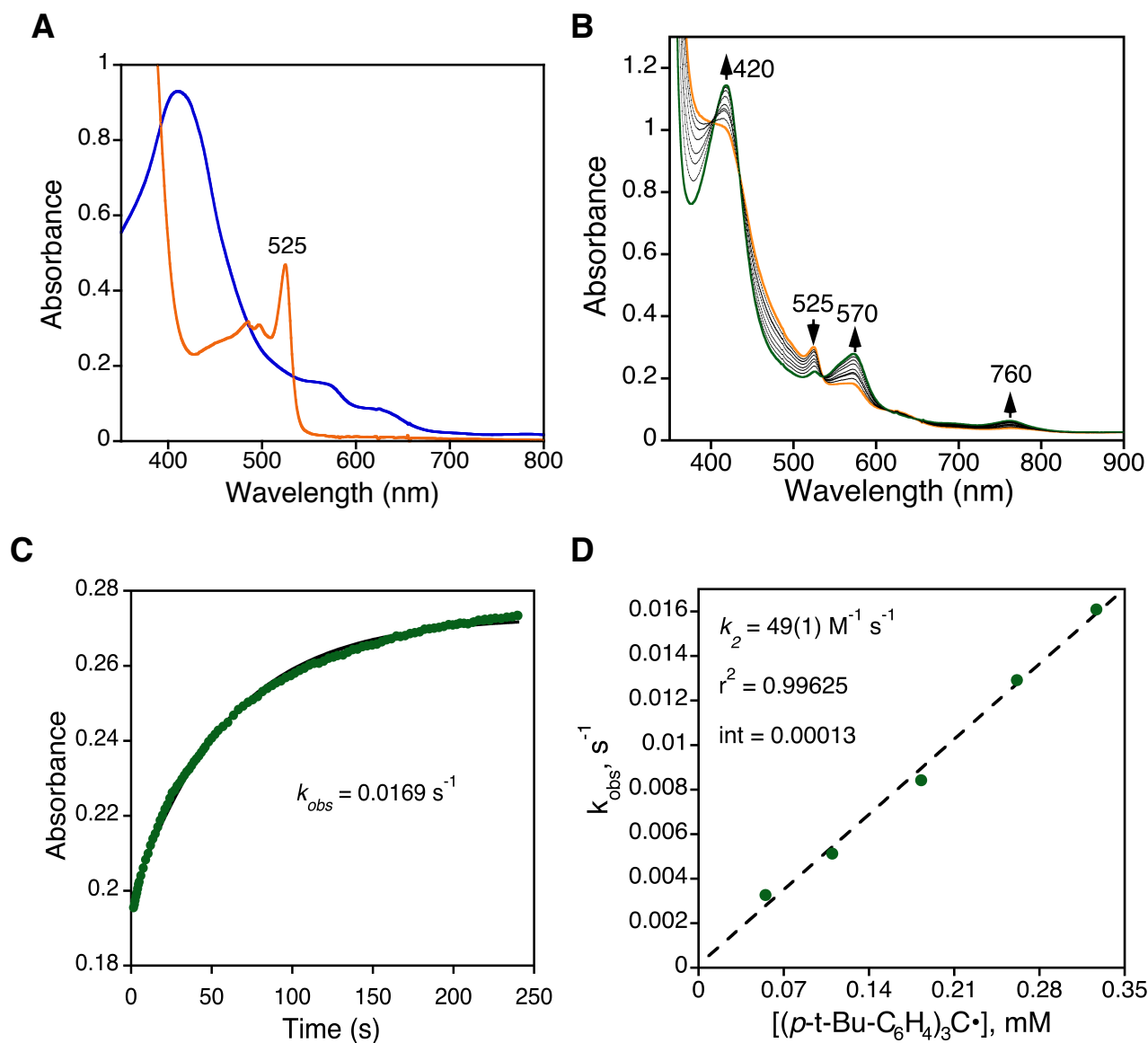


Fig. S18. a) Overlay of UV-vis spectra of **2** (blue) and $(p\text{-}t\text{-Bu-C}_6\text{H}_4)_3\text{C}\cdot$ (orange). b) Time-resolved UV-vis spectral changes for the reaction of **2** (20 μM) and $(p\text{-}t\text{-Bu-C}_6\text{H}_4)_3\text{C}\cdot$ (0.33 mM) in toluene at 23 $^\circ\text{C}$ (orange line, $t = 0.5 \text{ s}$) to form **3** (green line, $t = 220 \text{ s}$). c) Changes in absorbance vs time for the growth of **3** (570 nm) (green circles). d) Plot of k_{obs} versus $[(p\text{-}t\text{-Bu-C}_6\text{H}_4)_3\text{C}\cdot]$.

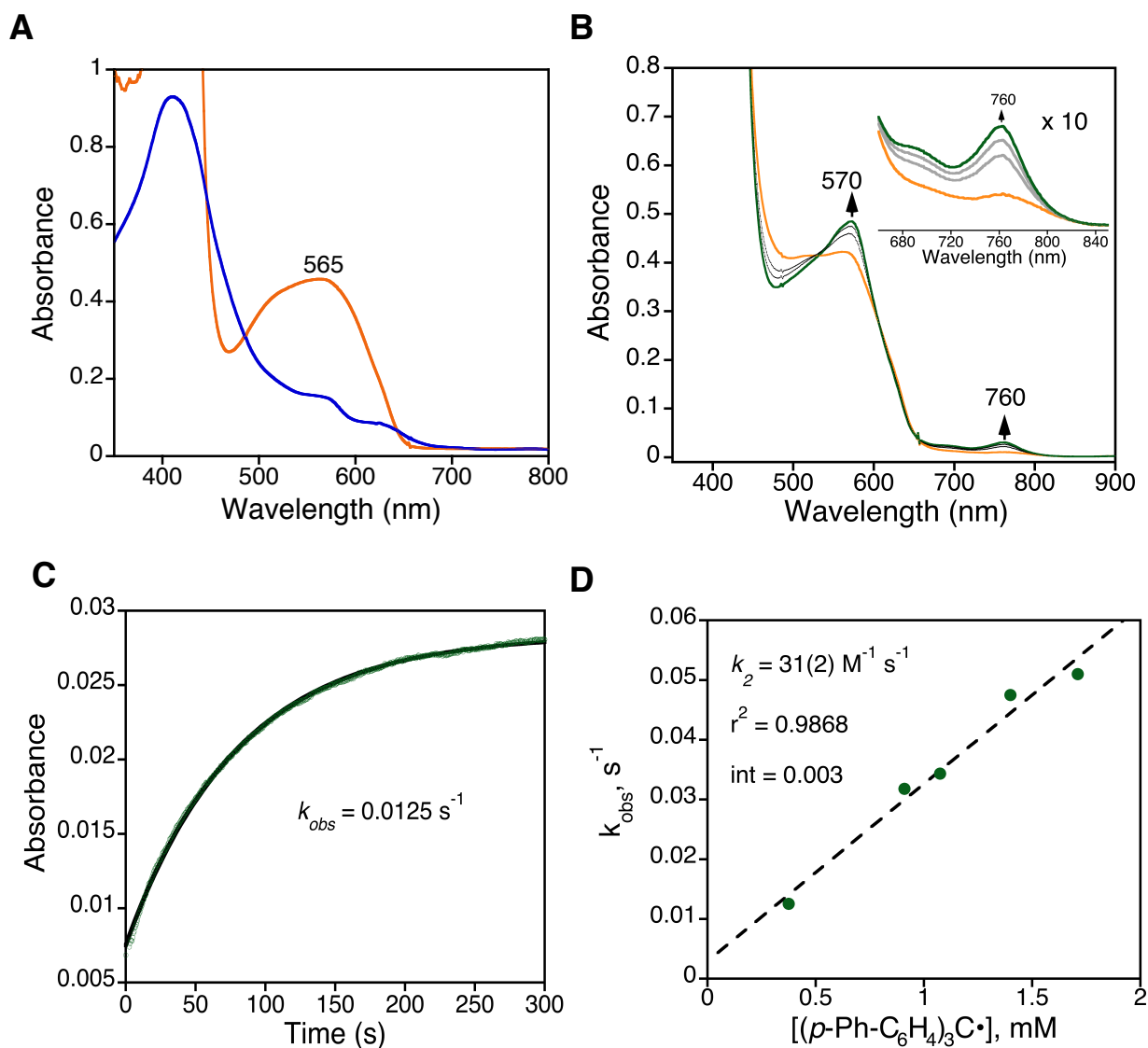


Fig. S19. a) Overlay of UV-vis spectra of **2** (blue) and $(p\text{-Ph-C}_6\text{H}_4)_3\text{C}\cdot$ (orange). b) Time-resolved UV-vis spectral changes for the reaction of **2** (20 μM) and $(p\text{-Ph-C}_6\text{H}_4)_3\text{C}\cdot$ (0.38 mM) in toluene at 23 $^\circ\text{C}$ (orange line, $t = 0.5$ s) to form **3** (green line, $t = 300$ s). c) Changes in absorbance vs time for the growth of **3** (760 nm) (green circles). d) Plot of k_{obs} versus $[(p\text{-Ph-C}_6\text{H}_4)_3\text{C}\cdot]$.

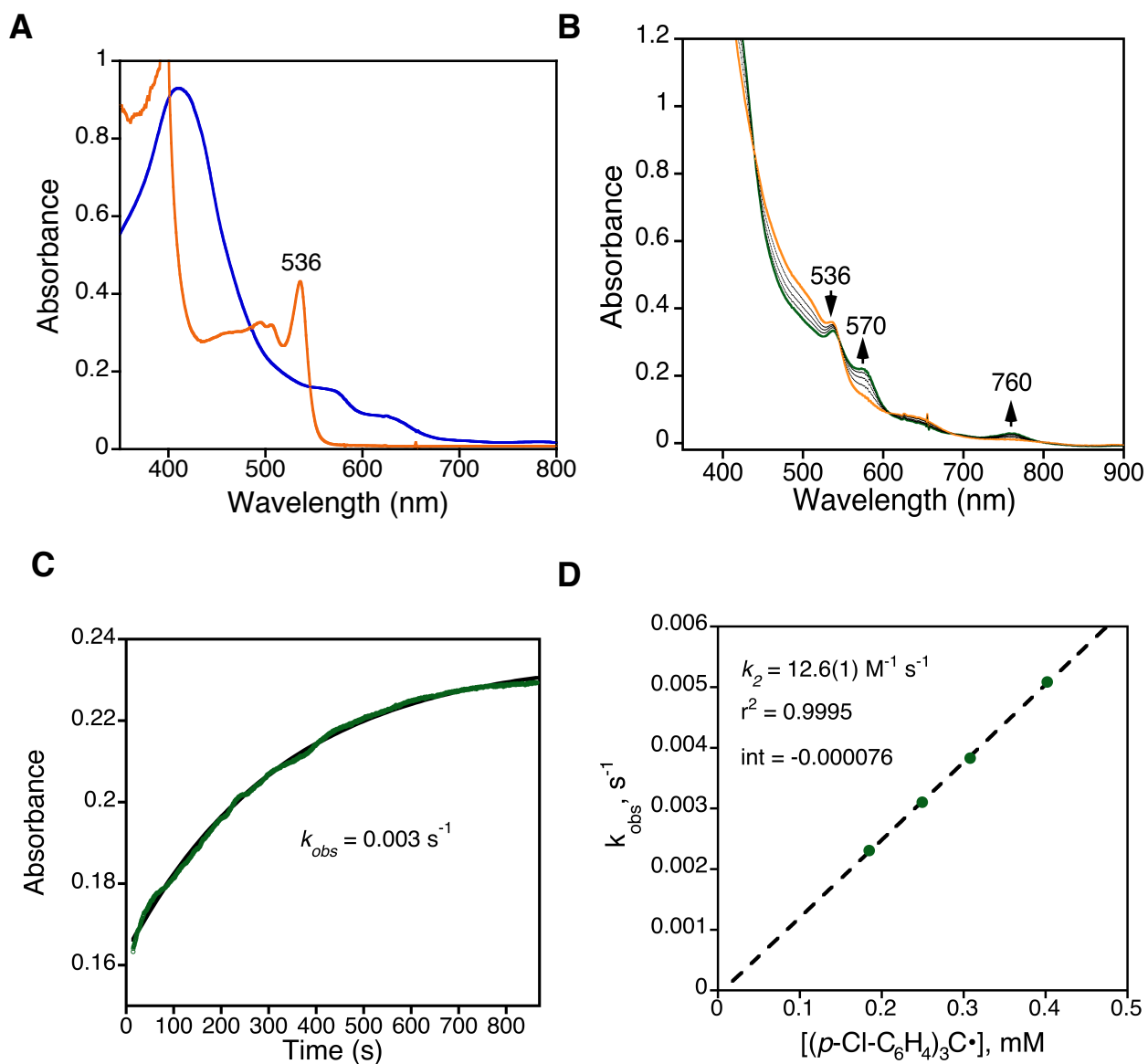


Fig. S20. a) Overlay of UV-vis spectra of **2** (blue) and $(p\text{-Cl-C}_6\text{H}_4)_3\text{C}\cdot$ (orange). b) Time-resolved UV-vis spectral changes for the reaction of **2** (20 μM) and $(p\text{-Cl-C}_6\text{H}_4)_3\text{C}\cdot$ (0.25 mM) in toluene at 23 $^\circ\text{C}$ (orange line, $t = 0.5$ s) to form **3** (green line, $t = 800$ s). c) Changes in absorbance vs time for the growth of **3** (570 nm) (green circles). d) Plot of k_{obs} versus $[(p\text{-Cl-C}_6\text{H}_4)_3\text{C}\cdot]$.

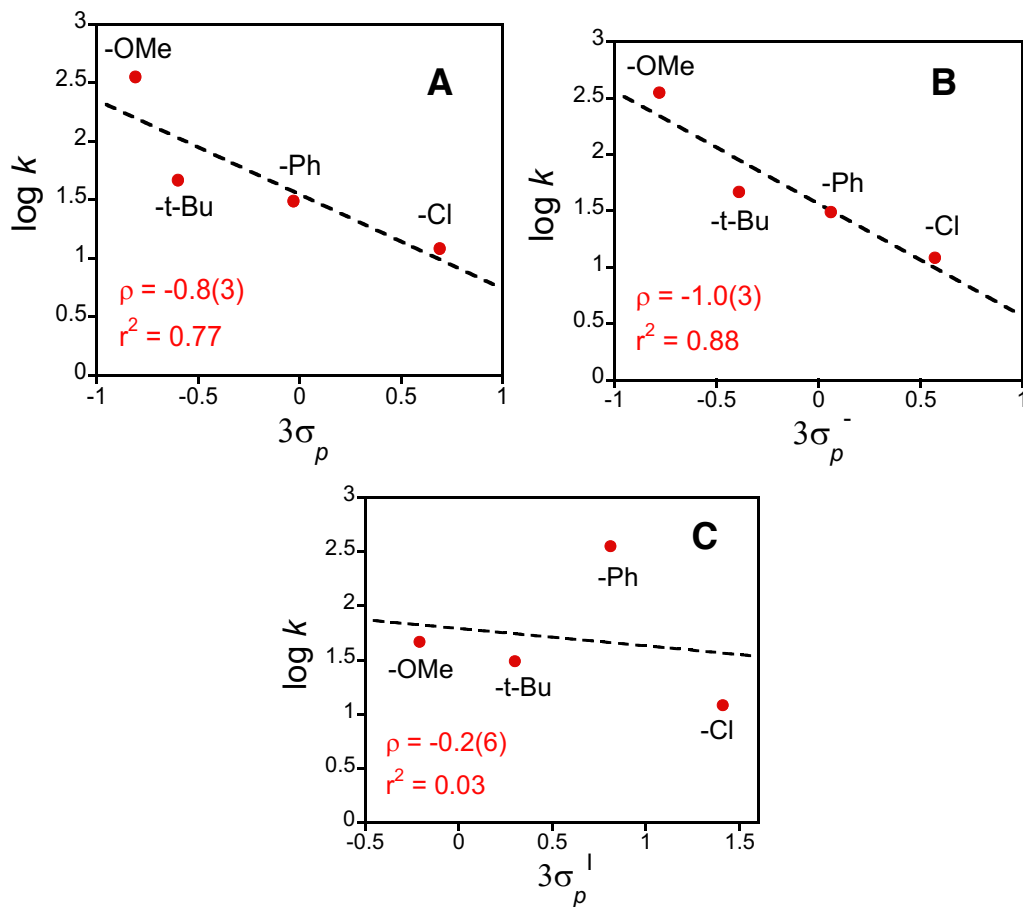


Fig. S21. Hammett plots using closed-shell σ parameters¹⁴: σ , σ^- , and σ^I . The slope and linear fits are also shown.

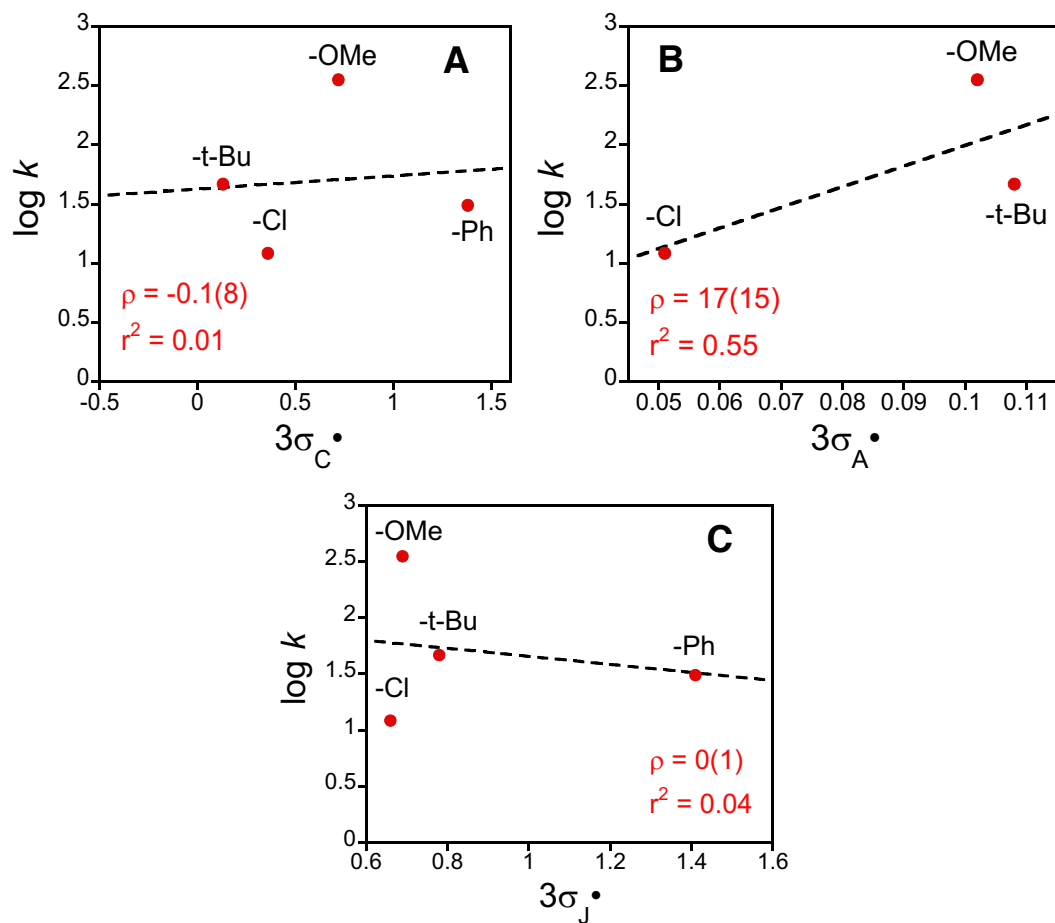


Fig. S22. Hammett plots using open-shell σ^* parameters defined by σ_C^* (Creary)¹⁷, by σ_A^* (Arnold)¹⁸, and σ_J^* (Jiang)¹⁹. The slope and linear fits are also shown.

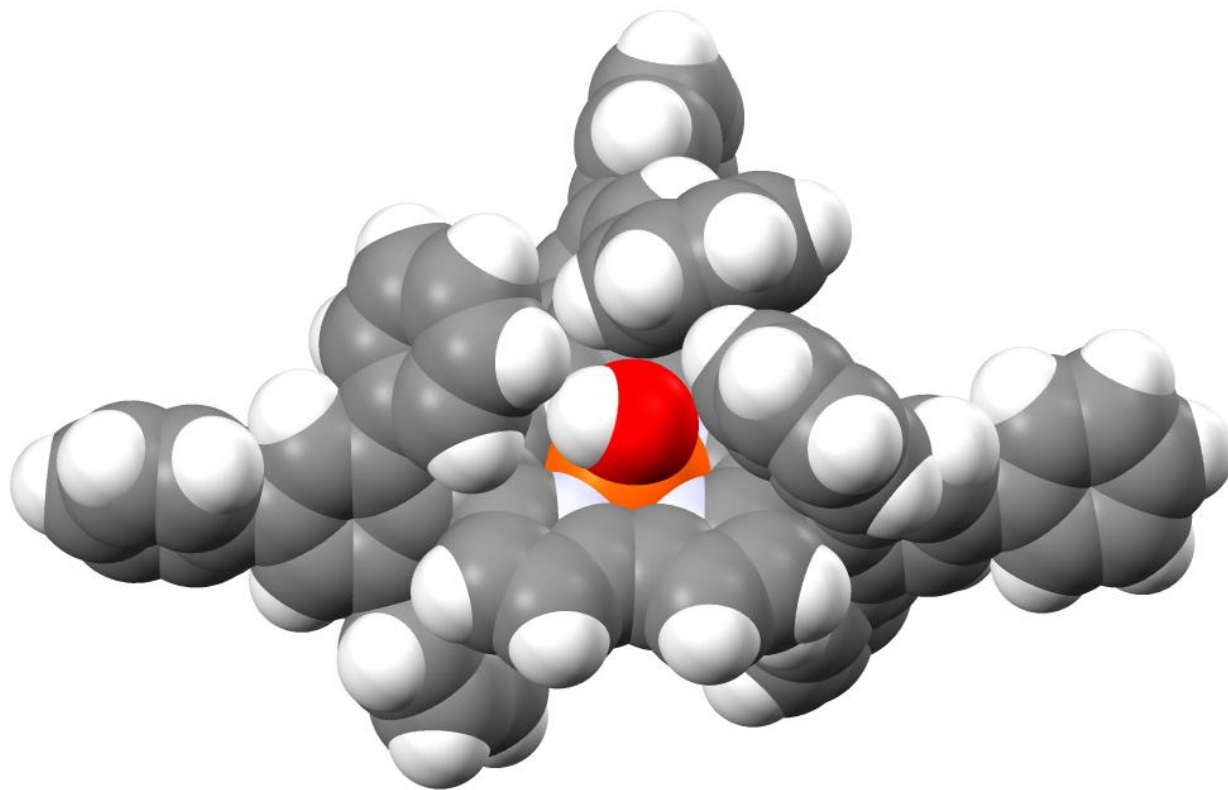
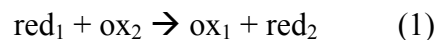


Fig. S23. Space-filling model for the molecular structure of **2** at 110(2) K.

Derivation of Marcus Plot Analysis²⁰⁻²¹

For a particular redox reaction (eqn 1):



the rate constant k_{12} can be formulated in terms of the free energy ΔG_{12}^\ddagger of the reaction:

$$k_{12} = Z_{12} e^{\frac{-\Delta G_{12}^\ddagger}{RT}} \quad (2)$$

$$\ln k_{12} = \frac{-\Delta G_{12}^\ddagger}{RT} + \ln Z_{12} \quad (3)$$

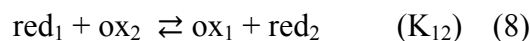
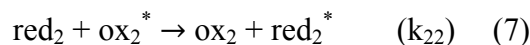
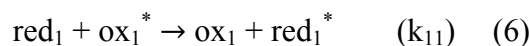
where Z_{12} is the collision frequency of 1 and 2 in solution, and ΔG_{12}^\ddagger is the sum of three terms: 1) electrostatic work to bring two ions together (ω_{elec}), 2) energy needed to modify the solvent structure ($\Delta G_{\text{solv}}^\ddagger$), and 3) energy needed to distort the metal-ligand bond-lengths ($\Delta G_{\text{lig}}^\ddagger$):

$$\Delta G_{12}^\ddagger = \omega_{\text{elec}} + \Delta G_{\text{solv}}^\ddagger + \Delta G_{\text{lig}}^\ddagger \quad (4)$$

For reactions involving an ion and a neutral molecule, ω_{elec} is 0. The solvent and ligand energy terms were quantified by Marcus,²² and this derivation led to the Marcus cross-relation:

$$k_{12} = (k_{11}k_{22}K_{12}f)^{1/2} \quad (5)$$

where k_{11} and k_{22} are rate constants for electron exchange between the oxidized and reduced states of an element (“self-exchange”), K_{12} is the equilibrium constant for the redox reaction between 1 and 2, and f is a function of k_{11} , k_{22} , and K_{12} .



$$\ln f = \frac{0.25 (\ln K_{12})^2}{\ln \frac{k_{11}k_{22}}{Z^2}} \quad (9)$$

Equation 5 can be re-written as:

$$\ln k_{12} = 0.5 \ln K_{12} + [0.5 \ln k_{11} + 0.5 \ln k_{22} + 0.5 \ln f] \quad (10)$$

The equilibrium constant K_{12} is then related to the standard redox potential E° by the Nernst equation:

$$\Delta G^\circ = -nRT \ln K = -nFE^\circ \quad (11)$$

$$\ln K = \frac{F}{RT} (E^\circ_{\text{red}} - E^\circ_{\text{ox}}) \quad (12)$$

Substituting equations 9 and 12 to equation 10 and keeping E°_{red} constant,

$$\frac{RT}{F} \ln k = -0.5 E^\circ_{\text{ox}} + \left[0.5 E^\circ_{\text{red}} + 0.5 \frac{RT}{F} \ln k_{11} + 0.5 \frac{RT}{F} \ln k_{22} + 0.5 \frac{RT}{F} \left(\frac{0.25 (\ln K_{12})^2}{\ln^2 \frac{k_{11} k_{22}}{z^2}} \right) \right] \quad (13)$$

where E°_{ox} is the redox potential of the substrate being oxidized. Under equilibrium conditions where $\Delta G^\circ \approx 0$ and $K_{12} \approx 1$, the last term in in eq 13 cancels out. Thus, under limiting conditions, the Marcus theory leads to a simple linear free energy relationship, where the slope of $(RT/F) \ln k$ versus E° is approximately -0.5 for reactions with an ET rate-determining step. The slope of -0.5 is expected only for cases where ΔG° is relatively small, because large values of ΔG° lead to an $\ln(f)$ term that is no longer ~ 0 . The slope of the Marcus plot approaches -1 for strongly endergonic reactions.²³

References

- (1) Aresta, M.; Nobile, C. F.; Petruzzelli, D., *Inorg. Chem.* **1977**, *16*, 1817.
- (2) Li, G.; Han, A.; Pulling, M. E.; Estes, D. P.; Norton, J. R., *J. Am. Chem. Soc.* **2012**, *134*, 14662.
- (3) Saito, S.; Nakazono, K.; Takahashi, E., *J. Org. Chem.* **2006**, *71*, 7477.
- (4) Broser, W.; Kurreck, H.; Niemeier, W., *Tetrahedron* **1976**, *32*, 1183.
- (5) Gomberg, M., *J. Am. Chem. Soc.* **1900**, *22*, 757.
- (6) Jang, E. S.; McMullin, C. L.; Käß, M.; Meyer, K.; Cundari, T. R.; Warren, T. H., *J. Am. Chem. Soc.* **2014**, *136*, 10930.
- (7) Liu, H.-Y.; Yam, F.; Xie, Y.-T.; Li, X.-Y.; Chang, C. K., *J. Am. Chem. Soc.* **2009**, *131*, 12890.
- (8) Dickie, D. A.; Jalali, H.; Samant, R. G.; Jennings, M. C.; Clyburne, J. A. C., *Can. J. Chem.* **2004**, *82*, 1346.
- (9) Dünnebacke, D.; Neumann, W. P.; Penenory, A.; Stewen, U., *Chem. Ber.* **1989**, *122*, 533.
- (10) Colle, T. H.; Lewis, E. S., *J. Am. Chem. Soc.* **1979**, *101*, 1810.
- (11) Sheldrick, G., *Acta Crystallogr., Sect. C* **2015**, *71*, 3.
- (12) Spek, A., *Acta Crystallogr., Sect. D* **2009**, *65*, 148.
- (13) Volz, H.; Lotsch, W., *Tetrahedron Lett.* **1969**, *10*, 2275.
- (14) Hansch, C.; Leo, A.; Taft, R. W., *Chem. Rev.* **1991**, *91*, 165.
- (15) Nakamoto, K., *Infrared and Raman Spectra of Inorganic and Coordination Compounds: Part A: Theory and Applications in Inorganic Chemistry*, Sixth ed.; John Wiley & Sons, Inc.: Hoboken, NJ, USA, 2008.
- (16) Sun, Z.-C.; She, Y.-B.; Zhou, Y.; Song, X.-F.; Li, K., *Molecules* **2011**, *16*, 2960.
- (17) Creary, X.; Mehrsheikh-Mohammadi, M. E.; McDonald, S., *J. Org. Chem.* **1987**, *52*, 3254.
- (18) Dust, J. M.; Arnold, D. R., *J. Am. Chem. Soc.* **1983**, *105*, 1221.
- (19) Jiang, X.; Ji, G., *J. Org. Chem.* **1992**, *57*, 6051.
- (20) Marcus, R. A.; Sutin, N., *Biochim. Biophys. Acta, Rev. Bioenerg.* **1985**, *811*, 265.
- (21) Brezonik, P. L., *Chemical Kinetics and Process Dynamics in Aquatic Systems*. Lewis Publishers: Boca Raton, Florida, 1993.
- (22) Marcus, R. A., *J. Phys. Chem.* **1963**, *67*, 853.
- (23) Wehrli, B., *Aquatic Chemical Kinetics*. Wiley-Interscience: New York, 1990.